Proton Pump Activity of Mitochondria-rich Cells
The Interpretation of External Proton-concentration Gradients

Lars J. Jensen,* Jens N. Sørensen,‡ E. Hviid Larsen,* and Niels J. Willumsen*

From the *Zoophysiological Laboratory, August Krogh Institute, The University of Copenhagen, DK-2100 Copenhagen Ø; and ‡Department of Fluid Mechanics, Building 404, Technical University of Denmark, DK-2800 Lyngby, Denmark

ABSTRACT We have hypothesized that a major role of the apical H^+-pump in mitochondria-rich (MR) cells of amphibian skin is to energize active uptake of Cl^- via an apical Cl^-/HCO_3^--exchanger. The activity of the H^+ pump was studied by monitoring mucosal $[H^+]$-profiles with a pH-sensitive microelectrode. With gluconate as mucosal anion, pH adjacent to the cornified cell layer was 0.98 ± 0.07 (mean ± SEM) pH-units below that of the lightly buffered bulk solution (pH = 7.40). The average distance at which the pH-gradient is dissipated was 382 ± 18 μm, corresponding to an estimated "unstirred layer" thickness of 329 ± 29 μm. Mucosal acidification was dependent on serosal pCO_2, and abolished after depression of cellular energy metabolism, confirming that mucosal acidification results from active transport of H^+. The $[H^+]$ was practically similar adjacent to all cells and independent of whether the microelectrode tip was positioned near an MR-cell or a principal cell. To evaluate $[H^+]$-profiles created by a multitude of MR-cells, a mathematical model is proposed which assumes that the H^+ distribution is governed by steady diffusion from a number of point sources defining a set of particular solutions to Laplace's equation. Model calculations predicted that with a physiological density of MR cells, the $[H^+]$ profile would be governed by so many sources that their individual contributions could not be experimentally resolved. The flux equation was integrated to provide a general mathematical expression for an external standing $[H^+]$–gradient in the unstirred layer. This case was treated as free diffusion of protons and proton-loaded buffer molecules carrying away the protons extruded by the pump into the unstirred layer; the expression derived was used for estimating stationary proton-fluxes. The external $[H^+]$-gradient depended on the mucosal anion such as to indicate that base (HCO_3^-) is excreted in exchange not only for Cl^-, but also for Br^- and I^-, indicating that the active fluxes of these anions can be attributed to mitochondria-rich cells.

KEY WORDS: active Cl^- transport • rheogenic H^+ pump • unstirred layer • mathematics of diffusion • proton concentration-profiles outside epithelial cells

INTRODUCTION

In amphibian epidermis, inward fluxes of Na^+ and Cl^- are coupled to cellular energy metabolism. Thus, these ions can be transported from a relatively dilute solution into the body fluids. This active uptake of Na^+ and Cl^- compensates for passive losses via the skin and distal renal epithelia. In the skin, as in collecting ducts and urinary bladder, several cell types are involved in the transcellular exchange of ions (reviewed by Steinmetz, 1986; Frömter, 1988; Larsen, 1991; Al-Awqati, 1992; Harvey, 1992; Kaissling and Stanton, 1992; Harvey, 1995; Brown and Stow, 1996; Gluck et. al., 1996). The most abundant cell type, the principal cells, constitutes the major pathway for active uptake of Na^+ accomplished by basolateral Na^+-K^+ ATPases in series with apical Na^+ channels. The other cell type, mitochondria-rich (MR)[1] or intercalated cells, can be divided into subpopulations serving different body functions. A common feature of MR cells is the expression of proton pumps. The H^+-pump activity and the anion fluxes through a coexpressed Cl^-/HCO_3^- exchanger are coupled to one another via the activity of a cellular carbonic anhydrase. In this way the H^+-pump can energize the elimination of a body acid-load (α-phenotype), the elimination of a body base-load (β-phenotype), or the rheogenic active uptake of chloride (γ-phenotype). The present investigation continues our studies on the active transport of Cl^- by the skin which seems to be brought about by a proton pump-driven uptake of Cl^- in exchange for cellular HCO_3^- (Larsen et. al., 1992; Larsen et al., 1996).

The activity of the apical H^+-pump can be studied by recording the mucosal $[H^+]$-gradient in the unstirred layer above the isolated epithelium. This method has been employed to localize functionally expressed rheogenic H^+-pumps to the apical membrane of MR-cells (Harvey, 1992; Larsen et al., 1992). In areas with few MR-cells, we applied the approximation of radial diffusion from point sources. In the present study we have elaborated a more general experimental and theoretical description of $[H^+]$-profiles generated by a large

Address correspondence to Lars Jørn Jensen, Zoophysiological Laboratory, Universitetsparken 13, DK-2100 Copenhagen Ø, Denmark. Fax: 45-3532-1567; E-mail: ljjensen@aki.ku.dk

[1]*Abbreviation used in this paper:* MR, mitochondria-rich.

number of MR-cells. We show that, generally, at any point above the cornified layer the $[H^+]$ is governed by so many MR cells that their individual contributions can not be experimentally resolved. We derive an expression for the external standing $[H^+]$–gradient for the case where free diffusion of protons and proton loaded buffer molecules carry away the protons pumped into the unstirred layer, and we discuss the application of this expression for estimating stationary proton fluxes. In addition, it is our aim to investigate the dependence of the external $[H^+]$-gradient on cellular energy metabolism and anion composition of the outside bath. Our results indicate that previously published active fluxes of Br^- and I^-, like those of Cl^-, can be attributed to transport systems of mitochondria-rich cells.

MATERIALS AND METHODS

Animals and Preparation

European toads (*Bufo bufo*) were kept in a terrarium at 20 ± 2°C with shelters, free access to tap water, and fed twice a week with mealworms ad lib. Toads used for experiments were killed during the intermoult period by double-pithing, and the skin was removed by dissection. The serosal side of the isolated skin was exposed for 1.5–2 h to a Ringer's solution containing 1.5–2 mg/ml Collagenase A (Boehringer Mannheim GmbH, Mannheim, Germany). The epithelium was then removed gently by use of a pair of forceps.

Electrophysiological Setup

The isolated epithelium was mounted mucosal side up in a mini-Ussing chamber (2 cm^2, own workshop) and bilaterally superfused with the desired solutions. The transepithelial potential (V_T) was measured via 200 mM-KCl/3%-agar bridges connected to a pair of calomel electrodes (Radiometer, Copenhagen, Denmark) matched to within <1 mV asymmetry. Short-circuit current (I_{SC}) was measured via chlorided silver-wires glued to the rim of each half-chamber. The total epithelial conductance (G_T) was calculated from the current response to a 10-mV V_T-pulse. Calomel and Ag/AgCl halfcells were connected to the headstage of a voltage-clamp circuit (VCC600; Physiological Instruments, San Diego, CA). The chamber was placed on the stage of an upright microscope (Optiphot-2 UD; Nikon, Tokyo, Japan). Apical borders of single MR-cells were easily distinguished from principal cells at 400× magnification (Nikon 40× water-immersion objective with Hoffman Modulation Contrast). Thus, with a micromanipulator (WR-60; Narishige, Tokyo, Japan) the tip of a microelectrode could be positioned directly above a selected cell. Via chlorided silver-wires, the double-barreled pH-sensitive microelectrode was connected to the headstages of a two-channel high input impedance electrometer (DUO 773; World Precision Instruments, Sarasota, FL). The pH-sensitive signal (V_{dif}) was recorded as the difference between the reference signal (V_{ref}) and the ion-sensitive signal (V_{ion}). The transepithelial potential and the microelectrode signals were measured with reference to the grounded mucosal bath, and recorded on a 5-channel pen recorder (Multipen Recorder; Rikadenki, Tokyo, Japan). The microscope with the mini-Ussing chamber, the microelectrode, and the headstages, was shielded by a Faraday cage and mounted on a vibration-isolated laboratory table (T-250.00; Physik Instrumente, Waldbronn, Germany).

Double-barreled pH-sensitive Microelectrodes

The microelectrodes were manufactured according to Willumsen and Boucher (1992). In brief, they were pulled on a horizontal microelectrode-puller (PD-5; Narishige) from two borosilicate glass capillaries (GC150 and GC120F; Clark Electromedical Instruments, Reading, UK) that were glued together longitudinally. The large diameter barrel (to become the ion-sensitive barrel) was silanized for 60–100 s with dimethyl-dichloro-silane (Fluka Chemie AG, Buchs, Switzerland) and subsequently baked for 1.5 h at 100°C. The tip of this barrel was backfilled with an ion-exchanger cocktail (Hydrogen ionophore II-Cocktail A, Fluka Selectophore #95297; Fluka Chemie AG). Both barrels were backfilled with 2-3 M KCl before use. The microelectrodes were calibrated before and after experiments in solutions of pH 6–8 and yielded a linear relationship with a Nernstian slope of 55.1 ± 0.4 mV/pH-unit ($N = 70$). To reduce electrical noise the microelectrode tips were broken in some experiments. Accordingly, the mean resistance of the two barrels was rather low, 52.5 ± 10.3 MΩ (reference-barrel, $N = 33$) and 57.1 ± 8.4 GΩ (pH-sensitive barrel, $N = 32$), respectively. Since the diameter of the broken tips never exceeded 1–2 μm, the electrodes were suitable for measuring pH-differences that occurred within the micrometer range. During experiments, the 90% rise-time of the pH-signal was <10 s. The hydrogen ionophore used in the present study is highly selective for protons over other cations, with Nicolsky-Eisenman selectivity coefficients in the range 4.1×10^{-9}–16×10^{-9} both for K^+:H^+ and Na^+:H^+ (manufacturer's information, Fluka Chemie AG, 1991) and for NH_4^+:H^+ (Willumsen and Boucher, 1992). Accordingly, we do not expect any influence of the major cations on the function of the proton-sensitive electrode barrel.

Solutions

Serosal (inside) control Ringer's buffered with CO_2/HCO_3^- contained (mM): Na^+ 115.2, K^+ 2, Ca^{2+} 1, Mg^{2+} 0.5, Cl^- 92, HCO_3^- 20, HPO_4^{2-} 2.8, CH_3COO^- 3, and pH was adjusted to 7.40 when bubbled with 95% O_2/5% CO_2. Mucosal (outside) Cl^--Ringer's contained (mM): Na^+ 111, K^+ 2, Ca^{2+} 1, Cl^- 111, SO_4^{2-} 2.1, Tris 0.1. All mucosal solutions were bubbled with 100% O_2 and pH adjusted to 7.40. In anion substitution experiments, Cl^- was replaced mole for mole by the impermeant gluconate, or by Br^- or I^-. A 2 mM Tris-buffered gluconate Ringer's was used in experiments in which the influence of the buffer capacity on the external $[H^+]$-gradient was investigated. Serosal CO_2 was eliminated by shifting to a mucosal type Cl^--Ringer's (see above) or a phosphate-buffered, CO_2/HCO_3^--free Ringer's containing (mM): Na^+ 115.2, K^+ 2, Ca^{2+} 1, Mg^{2+} 0.5, Cl^- 112, HPO_4^{2-} 2.8, CH_3COO^- 3, with pH adjusted to 7.40 when bubbled with 100% O_2. For reducing cellular ATP-pools, some epithelia were incubated for more than 12 h in serosal control Ringer's with 5 mM KCN, 1 mM 2-deoxy-glucose (Sigma Chemical Co., St. Louis, MO) and no CH_3COO^- added. Suppression of the ATP-level was also performed in the Ussing chamber in situ by exposing the epithelium to 5 mM mucosal KCN or 1 mM serosal 2-deoxy-glucose or bubbling serosal side with 95% N_2/5% CO_2 and the mucosal side with 100% N_2. The latter treatment was continued until a marked reduction of transepithelial potential was noted (>2 h).

Measurements of Mucosal pH-gradients

The epithelium was gently superfused on either side at a rate of ~1 ml/min. With mucosal and serosal chamber volumes of ~1 ml, the half-time for solution shifts is in the order of, $t_{1/2} \approx 40$ s. To facilitate the establishment of an acidified layer at the mucosal surface of the epithelium, the mucosal Ringer's was lightly

Tris-buffered (0.1 mM) and CO_2/HCO_3^--free. In this way we achieved a buffer capacity of the mucosal Ringer's solution at pH 7.40 of no more than 32.9 μM/pH-unit. This is about two orders of magnitude less than the buffer capacity of the standard serosal Ringer's solution of about 5 mM/pH-unit (pH = 7.40). The difference of pH between the epithelial surface and bulk solution was monitored as follows (Fig. 1). Under visual inspection, at 400× magnification, the tip of the pH-sensitive microelectrode was positioned directly above a selected MR- or principal cell. Generally, the cornified layer on top of the epithelium prevented us from positioning the microelectrode tip closer than 5–10 μm from the apical membrane of the selected MR cell.[2] When the pH-signal became stationary, the tip of the electrode was lifted 500 μm up into the bulk solution of fixed pH = 7.40. Accordingly, the "pH-gradient" was defined as ΔpH/500 μm and calculated as $\Delta V_{dif}/s$, where ΔV_{dif} is the change in pH-sensitive signal when the electrode was moved 500 μm upwards from the surface, and s is the slope of the pH-sensitive electrode's calibration curve. It follows that a positive pH-gradient indicates a lower pH at the epithelial surface than in the bulk solution.

[2]We did not measure the actual thickness of the cornified cell layer in vitro. The range indicated, 5–10 μm, is an estimate based on cryostat sectioned and acetone fixed specimens, e.g., Budtz et al. 1995.

Data Presentation

Results are given as mean ± SEM with the number of determinations (n, N) indicating total number of different cells above

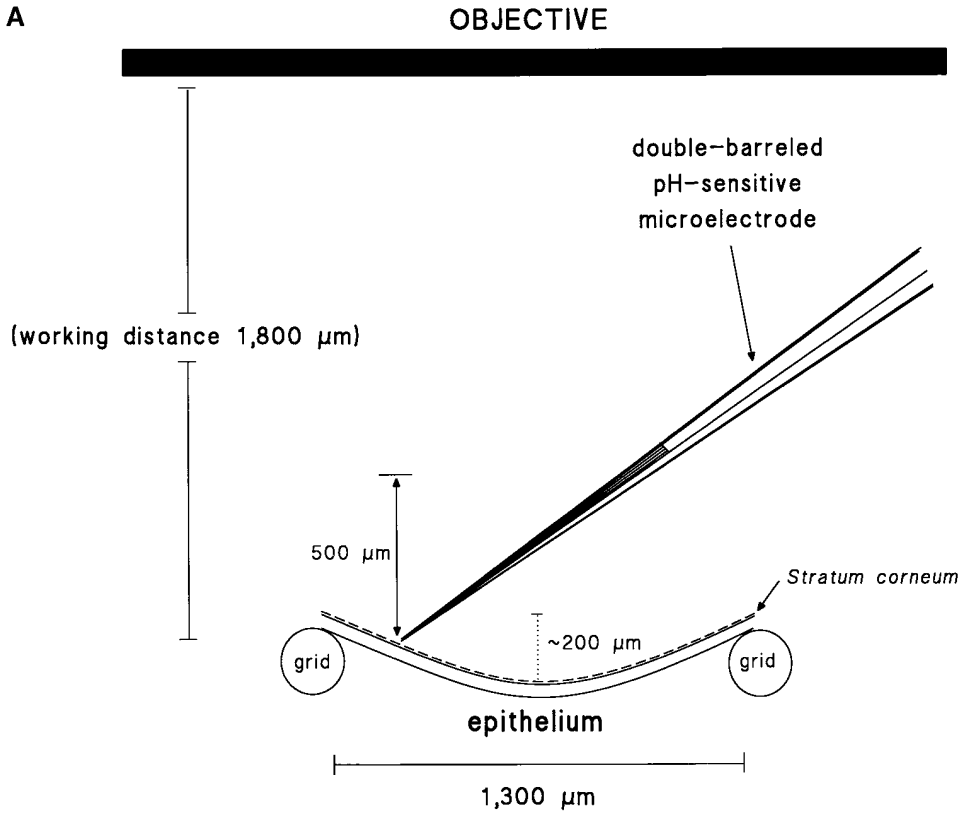

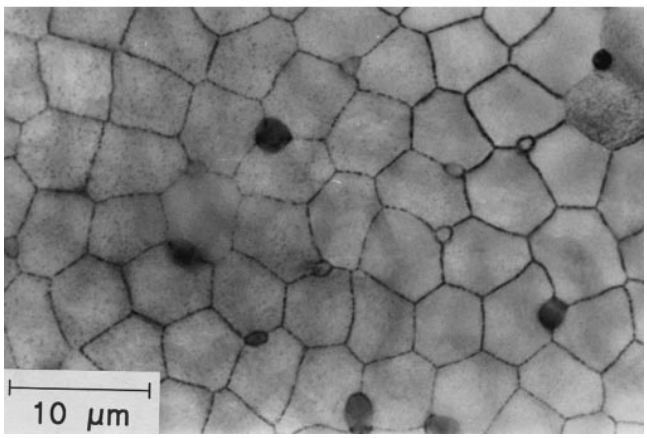

FIGURE 1. (*A*) Detection of standing pH gradients above the surface of the toad skin epithelium. The figure illustrates the geometry of the preparation when mounted on a supporting grid. The dimpling of the epithelium (concavities) is due to a slight negative hydrostatic pressure in the serosal half chamber. Approximately drawn to scale. (*B*) Top view of epithelium showing an uneven distribution of MR cells. After staining the skin with silver nitrate, the apical poles of the MR cells appear as dark spots.

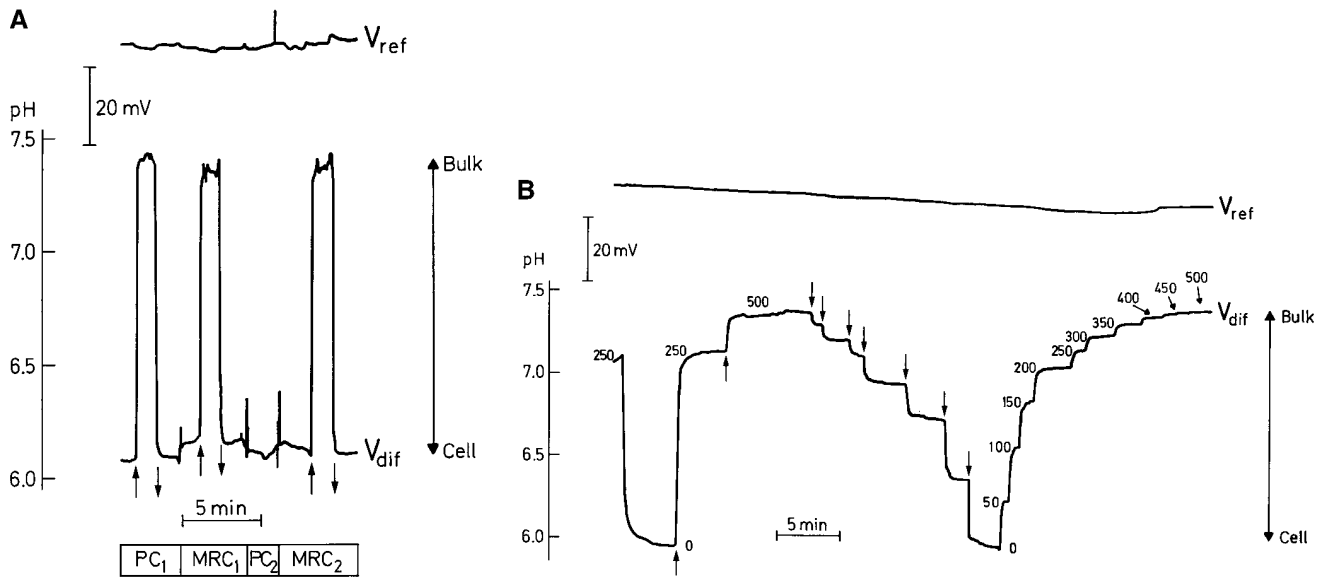

FIGURE 2. (*A*) Original tracings of local pH recorded with a pH-sensitive double-barreled microelectrode. The pH was determined from V_{dif} (*lower trace*) which is the difference between the pH-sensitive signal and the reference signal, V_{ref} (*upper trace*). Measurements were performed at the surface of the cornified cell layer (*Cell*) and in the mucosal bulk solution (*Bulk*), respectively, above either principal (*PC*) or mitochondria-rich cells (*MRC*). Vertical arrows indicate either upwards or downwards displacement of the microelectrode tip. Note, that in the case of PC_2, pH was measured at the surface, only. (*B*) Resolution of the mucosal pH gradient in vertical steps of 50 μm. Vertical arrows as in *A*. Numbers indicate the vertical distance from the microelectrode tip to the surface of the cornified cell layer.

which measurements were performed (n) and the number of animals (N) entering the experimental group, respectively. Unless otherwise stated, means were compared performing Student's (unpaired) t test (two populations with similar standard deviations, SD) or Welch's t test (different SDs). Levels of significance are indicated as two-tailed P-values and, when indicated, f is the degree of freedom.

RESULTS

Mucosal pH-gradients under Control Conditions

Original microelectrode recordings from experiments in which stationary pH-gradients were measured in the mucosal solution just above the isolated epithelium are shown in Figs. 2, *A* and *B*, 5, and 8. Under control conditions, with a Cl^--free solution superfusing the mucosal side of the preparation, the mucosal pH-gradient was always positive, i.e., the pH of the solution in the immediate vicinity of the epithelial surface was significantly lower than the pH of the bulk solution. In the fairly large number of experiments, the pH-gradient ranged from 0.17 to 2.57 with a mean of 0.98 ± 0.07 pH-U/500 μm (n = 249, N = 57). The mean number of cells investigated in preparations with gluconate outside was 4.4 ± 0.3, ranging from 1 to 13 cells per preparation. While the mucosal pH-gradient varied significantly among the preparations, the variation among different MR-cells within a given preparation was insignificant. Accordingly, a one-way Anovar test gave an F-value of 5.33 indicating that the variance of measurements from different preparations was significantly higher than the variance of measurements within individual preparations (F is the ratio between these two variances; $P < 0.0001$, $n = 129$, $N = 23$).

The horizontal pH profile. The pH-recordings shown in Fig. 2 *A* were performed above a principal cell and two MR cells (the pH-gradient above the second principal cell, PC_2, was not monitored). There was no significant difference in the magnitude of the pH-gradient measured above the principal cell and the MR cells, respectively. This result was obtained for all preparations independent of the mucosal [Cl^-] (Cl^--free: $P = 0.94$, $N = 9$, or, 111 mM Cl^-: $P = 0.12$, $N = 7$; paired t test), and it was independent of the mucosal chamber perfusion rate. Furthermore, by moving the pH-sensitive microelectrode in a horizontal direction, we scanned the horizontal pH-profile at a distance of 1–5 μm above the preparation. This method also failed to show variations of pH above the different cell types.

The vertical pH profile. Figs. 2 *B* and 8 show examples of the vertical pH profile in the solution above the toad skin epithelium. The original microelectrode recordings in these figures also indicate how the profile was experimentally determined. With the tip of the pH-sensitive microelectrode as close as possible to the cornified layer above an MR-cell, pH was recorded until a stationary value was obtained. Subsequently, the tip was carefully moved upwards in steps of 50 μm and the stationary pH recorded at each position. In these examples, the total gradient was ~1.5 pH-U/500 μm. However, it can also be seen that already at a position of

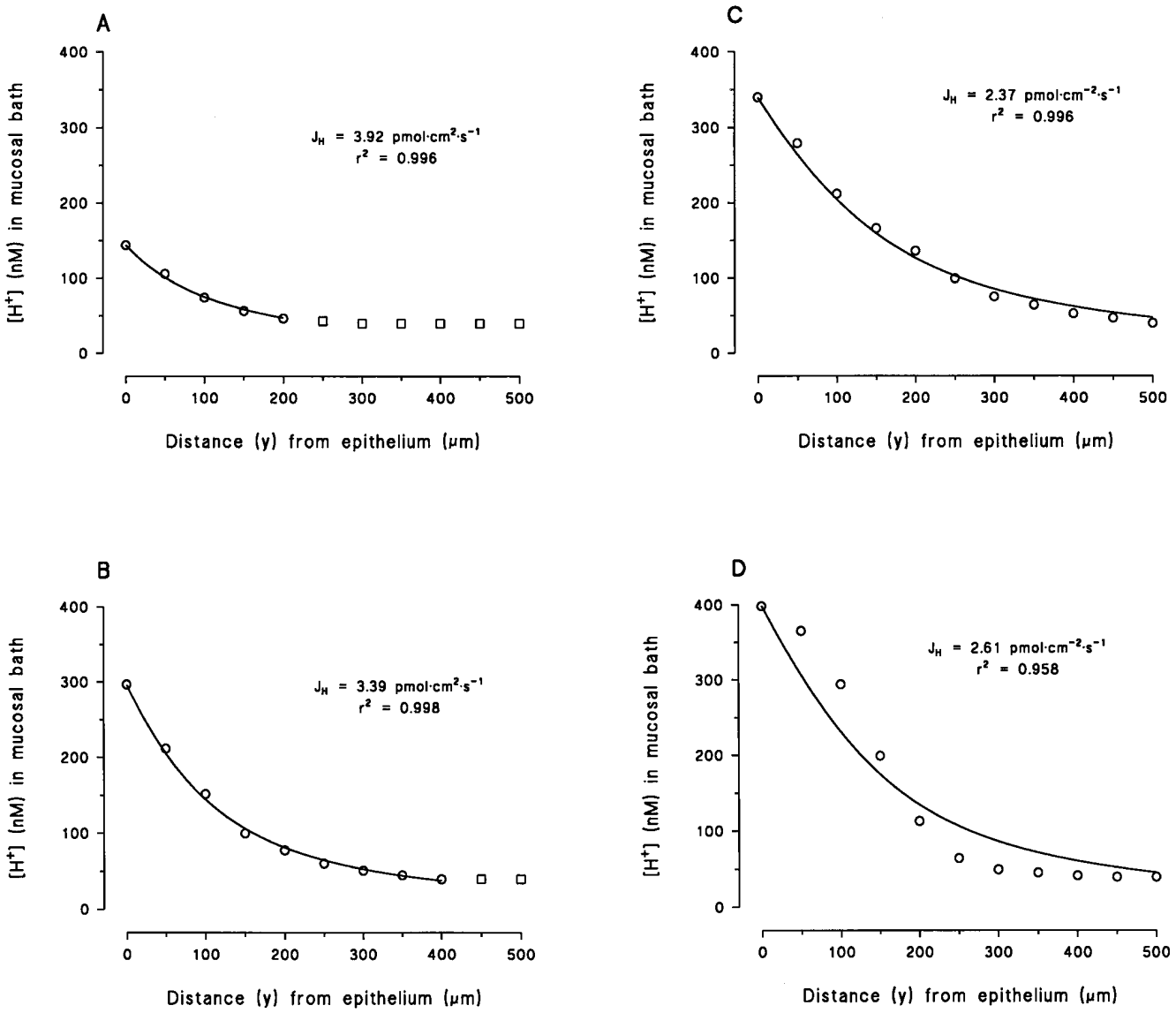

FIGURE 3. Vertical $[H^+]$-profiles in mucosal bath. Full lines represent best fit to the data by Eq.(4) based on a mathematical model developed for determination of the proton flux (see DISCUSSION and APPENDIX B). (*A–C*) Typically, data were well fitted by Eq. 4. The theoretical line deviates from the data at various distances from the surface (the point where the full line ends), indicating variation of the thickness of an unstirred (diffusion) layer. (*D*) Occasionally, data were obtained which were poorly fitted by Eq. 4.

350–400 μm above the surface of the epithelium the pH gradient had fully dissipated, i.e., the pH was identical to that of the buffered bulk solution. The average vertical distance (y) at which the pH-gradient had dissipated was 382 ± 18 μm ($N = 22$). From these measurements the vertical $[H^+]$-profiles could be depicted. Fig. 3, *A–D* shows typical examples of $[H^+]$-profiles. Full lines are curvefits based on a mathematical model allowing us to calculate the net efflux of protons from the epithelium (see DISCUSSION).

Effects of stirring and mucosal buffer capacity. We would expect that the pH-gradient in the mucosal solution above the preparation depends on the following three factors, (*a*) the rate of proton secretion by the cells, (*b*) the rate at which the mucosal chamber is being perfused, and (*c*) the buffer capacity of the mucosal perfusate. Fig. 4 shows the effect of varying perfusion rate and buffer concentration. As expected, the pH-gradient was significantly reduced, by 35% ($P < 0.05$, $N = 7$; paired t test), when the mucosal perfusion rate was doubled. Likewise, a 20-fold increase in the buffer concentration of the mucosal bath resulted in a reduction of 68% ($P < 0.01$, $N = 4$; paired t test) of the pH-gradient above the preparation (Fig. 4). To obtain a measurable external pH-gradient, the perfusion rate and the buffer capacity were constantly kept low.

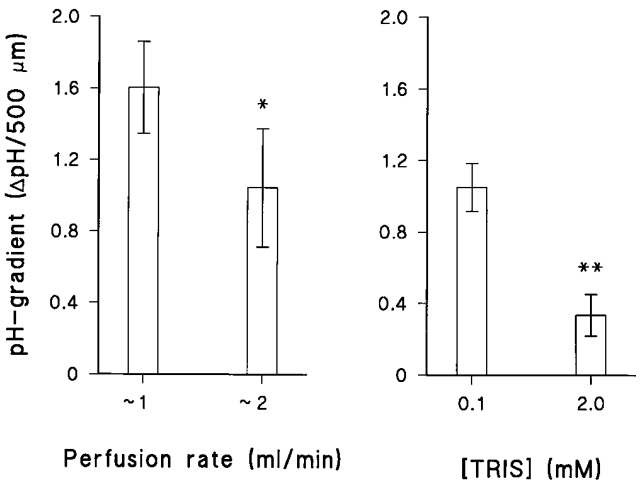

FIGURE 4. Effects of varying perfusion rate (*left*) and buffering capacity (*right*) of the mucosal medium on the magnitude of the pH gradient. * and ** indicate $P < 0.05$ and $P < 0.01$, respectively.

Substrate Requirements of the Apical Proton Pump

Effect of CO_2 depletion. MR cells are especially rich in the enzyme carbonic anhydrase (Rosen and Friedley, 1973) which catalyzes the hydration of CO_2 to H_2CO_3. Subsequently, the carbonic acid is dissociated into H^+ and HCO_3^-. It is our hypothesis that the activity of the apical proton ATPase, which pumps protons from the cell into the mucosal solution, depends on H^+ from the carbonic anhydrase–mediated hydration of CO_2. Since CO_2 readily diffuses through the amphibian skin, however, the source of CO_2 is possibly not only the metabolic processes of the skin, but also the large CO_2-pool of the serosal bath. Fig. 5 shows that elimination of CO_2 from the serosal bath resulted in a significant reduction of the mucosal pH-gradient. After reintroduction of CO_2, the mucosal pH-gradient always recovered fully (not shown). Mean values of the stationary pH-gradients in the presence and absence of external CO_2, respectively, are given in the left panel of Fig. 6. The difference between pH-gradients obtained with Tris-buffered (0.1 mM, $N = 10$) and phosphate-buffered (2.8 mM HPO_4^{2-}, $N = 6$) CO_2-free serosal solutions, respectively, was not statistically significant ($P = 0.18$). Thus, a relatively high pCO_2 of the serosal bath is of major significance for maintaining large mucosal pH-gradients. In both groups (Fig. 6, *left*), the small mucosal pH-gradient observed with CO_2-free serosal solution is significantly different from zero ($P < 0.0005$, $N = 16$; one-sample t test) suggesting, therefore, that there is a residual proton secretion due to the metabolic CO_2 production of the tissue. By measuring the current generated by the proton pump, a similar small activity was noted after removal of CO_2 from the bathing solutions (Larsen et al., 1992). It is of further interest that the time-course of the alkalization of the mucosal solution adjacent to the cornified cells after removal of serosal CO_2 had a half-time of $t_{1/2} = 252 \pm 78$ s, ($N = 7$), which is much slower than the time-course of the serosal solution-shift, governed by a half-time of ~40 s. This delay might be explained by assuming an effect of a serosal unstirred layer, so that the diffusion of CO_2 to/from

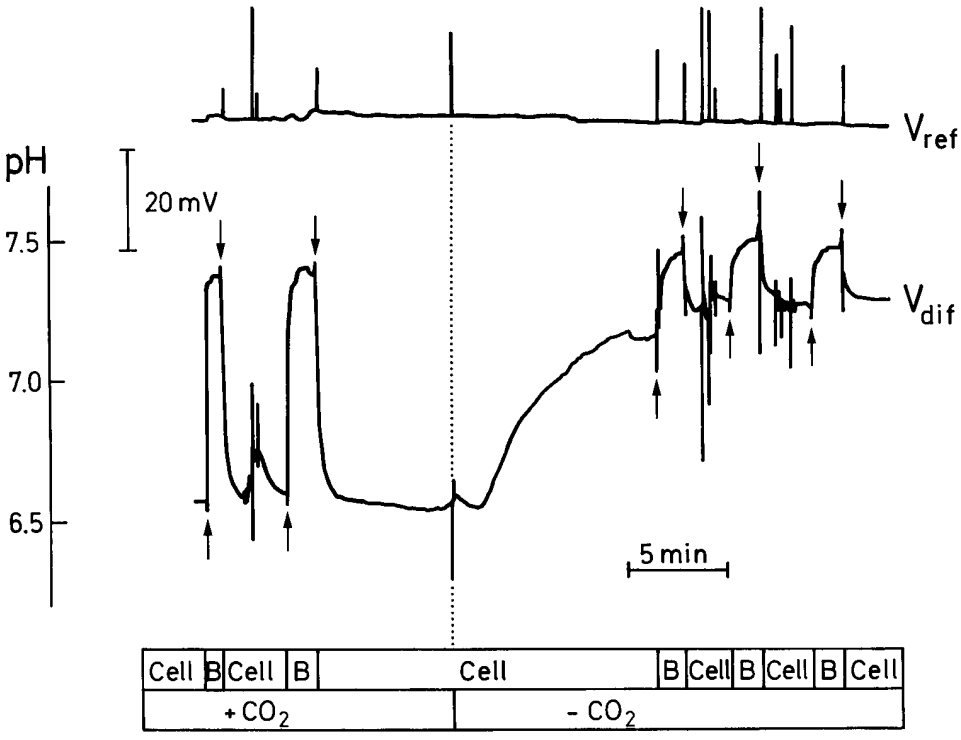

FIGURE 5. The effect of eliminating CO_2 from the serosal perfusate on the magnitude of the mucosal pH gradient. Vertical dotted line locates the onset of a solution shift. *Cell* and *B* denote positions of the microelectrode tip at the surface of the cornified cell layer and in the bulk solution, respectively. Vertical arrows as in Fig. 2.

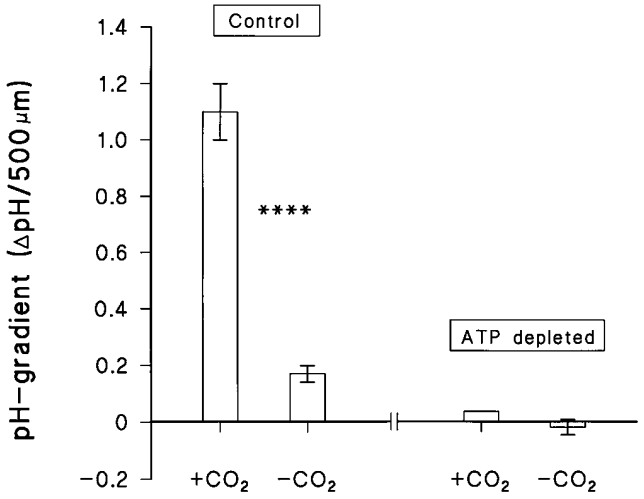

FIGURE 6. Summary of experiments in which serosal CO_2 was eliminated in the presence of normal (*Control*) and reduced (*ATP depleted*) intracellular ATP concentrations. ****$P < 0.0001$.

the MR cells would become the rate-limiting step. However, a redistribution time, t_{red} (Sten-Knudsen, 1978), of 252 s for the [CO_2]-profile to reach steady state would require an unstirred layer thickness of 1,194 μm, which seems unrealistic in our chamber. The thickness of the serosal unstirred layer, therefore, can only partially account for the time course of mucosal alkalization following removal of serosal CO_2. Thus, apart from being substrate for the carbonic anhydrase, there may be another mechanism for CO_2 to exert control over proton secretion, e.g., by regulating the number of active proton pumps in the membrane. In turtle urinary bladder CO_2 stimulates exocytosis of vesicles containing H^+ pumps on a time scale of minutes (Gluck et al., 1982).

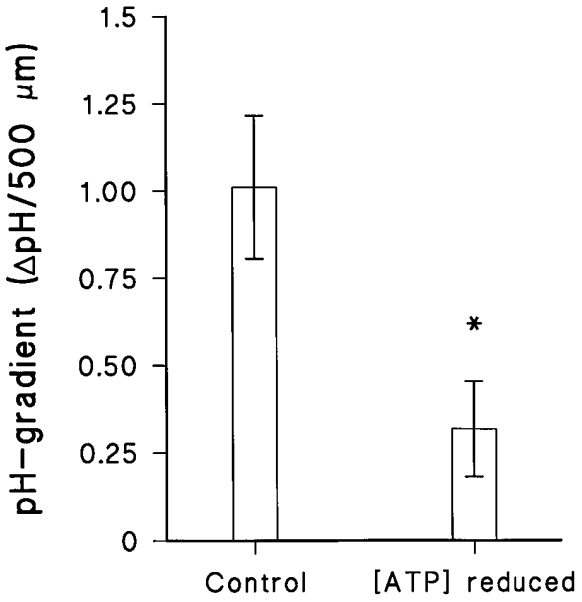

FIGURE 7. The effect of reduction of cellular ATP concentration on mucosal pH gradients. *$P < 0.05$.

Effect of depression of cellular energy metabolism. Figs. 6 and 7 present the results of experiments in which we attempted to deplete the epithelial cells for ATP. In one group of experiments (Fig. 7), the cellular energy metabolism was experimentally reduced after the preparation had been mounted in the Ussing-chamber by exposure to N_2-equilibrated solutions containing 5 mM CN^- and 1 mM 2-deoxy-glucose (MATERIALS AND METHODS). As judged from a resulting submaximal reduction in transepithelial potential (63 ± 22%, $N = 5$, not shown), even after 2 h exposure to these conditions, only a partial depletion of the cellular ATP-pool was achieved. Nevertheless, when comparing the pH-gradients measured prior and subsequent to the above mentioned treatment, the pH-gradient in the partially ATP-depleted preparations was statistically reduced ($P < 0.05$, $f = 4$; $N = 5$; $n = 18$ cells). In these experiments with a steep transepithelial CO_2-gradient, we cannot exclude the possibility that transepithelial diffusion of CO_2 from the serosal (5% CO_2) to the mucosal solution (nominal CO_2-free) contributed to the acidification during the

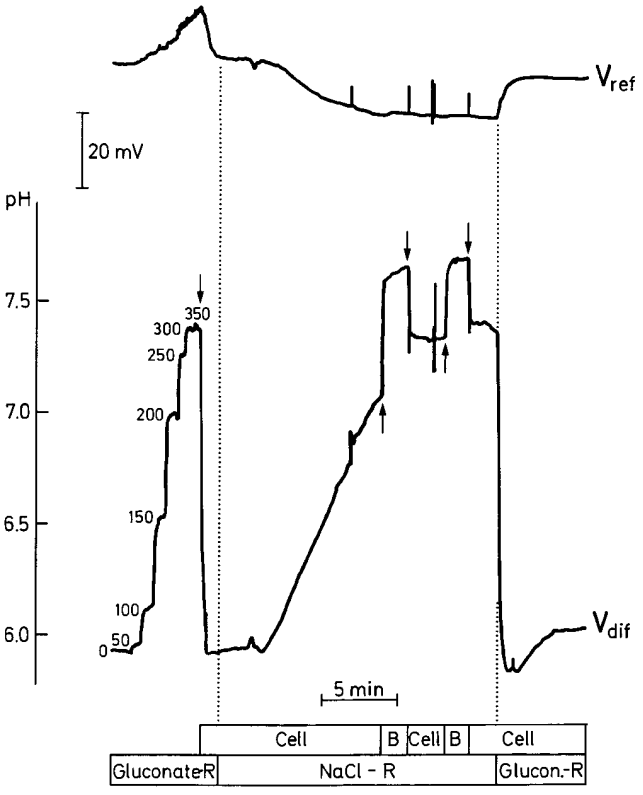

FIGURE 8. Effect of changing the major anion in the mucosal perfusate from 111 mM gluconate (*Gluconate-R*) to 111 mM Cl^- (*NaCl-R*) on the mucosal pH gradient. The figure illustrates that in the presence of Cl^- in the mucosal bath, the pH gradient is strongly reduced. Before the introduction of Cl^- the vertical pH profile was resolved as explained in the legend to Fig. 2 *B*. Vertical dotted lines and arrows as in Figs. 2 and 5.

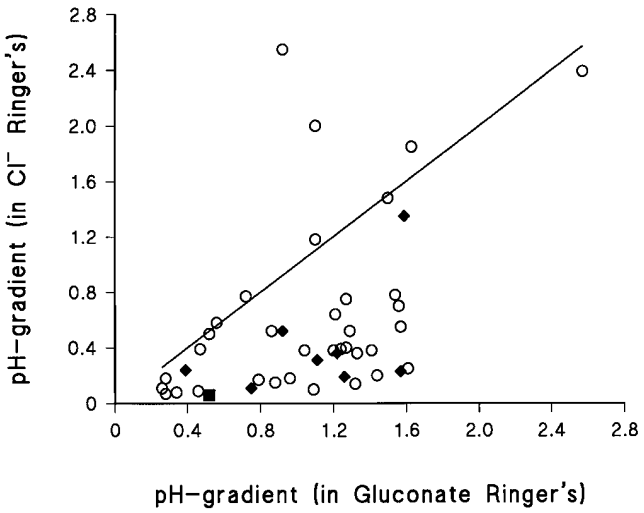

FIGURE 9. Summary of all experiments (N = 43 animals) in which pH gradients were measured with Cl^- and gluconate as major mucosal anion, respectively. Measurements were performed under short-circuit conditions (○), open-circuit conditions (◆), or under open-circuit conditions in the presence of 0.1 mM mucosal amiloride (■).

initial control period. Therefore, in the second group of experiments (Fig. 6, *right*) we investigated the effect of a similar pulsing of serosal CO_2 on the mucosal pH-gradients in preparations which had been almost fully ATP-depleted before mounting in the Ussing-chamber (MATERIALS AND METHODS). On the average, the mucosal pH-gradient measured in these ATP-depleted epithelia exposed to a CO_2-free serosal solution was -0.018 ± 0.027 (n = 8) and when CO_2/HCO_3^- was introduced, the pH-gradient increased to 0.0378 ± 0.0003 (n = 10; the change was NS, $P = 0.29$, $N = 2$). Furthermore, the reduction of the mucosal pH-gradient after removal of serosal CO_2 is significantly smaller in fully ATP-depleted preparations than in control preparations ($P < 0.01$; $f = 16$). These results confirm that the proton concentration gradient in the mucosal solution depends entirely on active transport rather than being maintained by transepithelial diffusion of CO_2.

Mucosal Anion Substitutions

Replacement with chloride. Fig. 8 shows a microelectrode recording which demonstrates the effect of replacing mucosal gluconate with chloride on mucosal acidification. As discussed above, prior to the replacement of gluconate, the vertical pH-profile was recorded by moving the tip of the microelectrode upwards in steps of 50 μm. Subsequently, Cl^- was introduced in the mucosal bath and a pronounced alkalization was detected at the surface of the cornified cells above an MR cell. At the new steady state, the pH-gradient was significantly reduced. After reintroduction of gluconate, the MR cell again acidified the mucosal solution, illustrating that the alkalinizing effect of mucosal chloride ions is reversible. The average response to shifting between gluconate and Cl^--Ringer's was a highly significant reduction of the pH-gradient from 1.08 ± 0.07 (n = 199) to 0.59 ± 0.09 (n = 134) pH-U/500 μm ($P < 0.0001$, N = 43) The range of pH-gradients in Cl^--Ringer's was 0.06–2.57 pH-U. The mean number of cells investigated per preparation was 3.1 ± 0.4, ranging from 1 to 10 cells per preparation.

Reproducibility of results. Within each preparation, all cells studied showed the same type of response. How-

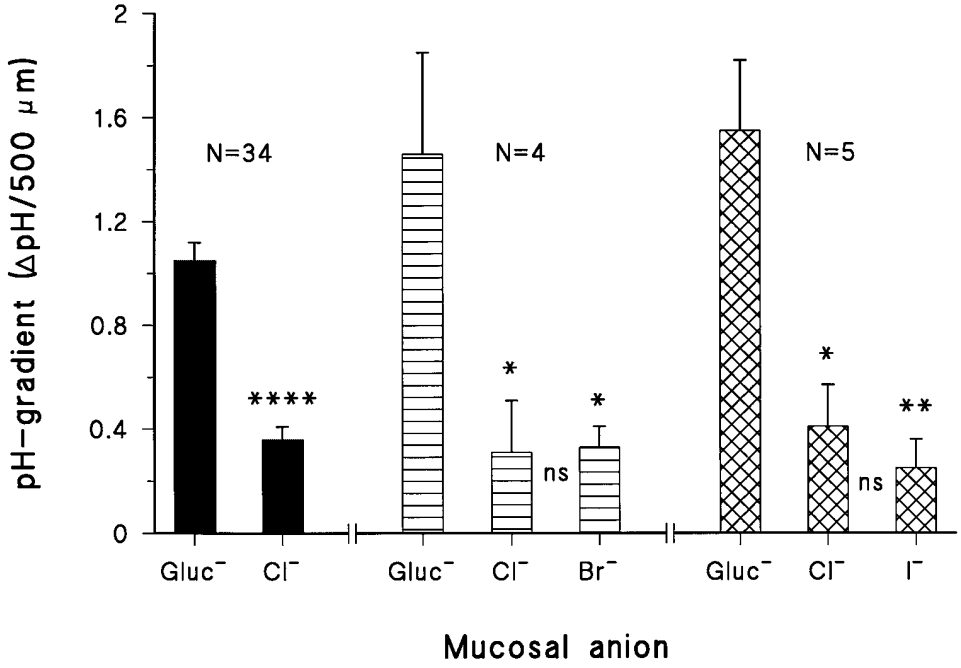

FIGURE 10. Effect of substitution of mucosal gluconate with Cl^-, Br^-, and I^-, respectively, on the mucosal pH gradients. The symbols *, **, ****, and *ns* indicate $P < 0.05$, $P < 0.01$, $P < 0.001$, and no significance, respectively.

ever, in 9 out of 43 preparations the pH-gradient measured in gluconate-Ringer's was not different from that measured in Cl^--Ringer's, i.e., a shift from 1.18 ± 0.22 to 1.48 ± 0.26 pH-U/500 μm was observed ($P = 0.39$, $N = 9$). Fig. 9 summarizes the results obtained from the individual preparations. Here, points on and above the line of identity represent preparations which did not respond with local alkalization to a shift from mucosal gluconate to Cl^-. In the preparations that did respond (points below the line of identity), the pH-gradient was reduced from 1.05 ± 0.07 to 0.36 ± 0.05 pH-U/500 μm ($P < 0.0001$, $N = 34$, see also Fig. 10, *left*). The experimental period covered all seasons of the year. Nevertheless, it is noteworthy that seven of the nine preparations which did not respond by alkalization to the addition of external Cl^- were studied during a 1 month mid-summer period.

Replacement with bromide and iodide. We compared the above result obtained by replacing gluconate with Cl^- with the effect of introducing either Br^- or I^- as the major anion in the mucosal bath. Fig. 10 shows the effect of such anion substitutions on the stationary pH-gradient. It can be seen that all of the three halides tested produced a significant decrease in the mucosal pH-gradient (the results of the statistical treatments are given in the associated figure legend). After reintroduction of gluconate in the mucosal solution, the pH-gradient was always reestablished. In other words, the alkalinizing effect of the halides was fully reversible.

DISCUSSION

With gluconate as major anion in the mucosal bath, we found that the steady-state pH in the unstirred layer just above the surface of the short-circuited toad skin epithelium was 0.98 ± 0.07 ($N = 57$) pH-units below that of the bulk solution (pH = 7.40). This $[H^+]$-gradient was very significantly reduced in response to cellular ATP-depletion (Fig. 7). These observations indicate that mucosal acidification depends on cellular energy metabolism rather than on a passive distribution of protons governed by the transepithelial electrical potential difference or the preestablished transepithelial CO_2/HCO_3^--gradient. Thus, the inhibition of mucosal acidification in response to reduction of serosal pCO_2, which is another clear result of the present study (Figs. 5 and 6), is most likely caused by depletion of cellular CO_2 as substrate for the epithelial carbonic anhydrase providing H^+ to the apical proton-ATPase. In the frog skin, carbonic anhydrase activity has been demonstrated in the MR cells, exclusively (Rosen and Friedley, 1973). The H^+-flux can be inhibited by the proton-pump inhibitors DCCD (dicyclohexyl-carbodiimide, Harvey, 1992), Bafilomycin and Folimycin (Klein et al., 1995), thus, providing pharmacological evidence for a V-type proton-ATPase in the epidermal MR cells. In agreement with this hypothesis, Klein et al. (1995) found immunocytochemical fluorescent signals located in MR cells in frog skin exposed to fluorescent V-ATPase antibodies.

Accordingly, we expect that it is the secretion of protons by MR cells at a steady rate into the unstirred layer on the outside of the epithelium which provides the source from which protons diffuse into the superfusing solution. In principle, therefore, the external proton concentration-gradient builds up as a result of radial diffusion from an array of "point sources." Nevertheless, our present study indicated that the measured external proton concentration profile resembles that of a plate source. Intuitively, with a large number of mitochondria-rich cells, one might expect that these two cases — the "multiple point source" versus the "homogeneous plate source" — are indistinguishable at some distance from the surface containing the source(s). To provide theoretical support for this notion, what follows first is an analysis of a mathematical model of $[H^+]$-profiles created by a number of point sources from which protons diffuse into a sink located at infinite distance from the sources. To compare the proton pump activity of our preparation with previously directly measured active fluxes of H^+, we next derive expressions which can be used for calculating the flux from measured $[H^+]$-gradients. Finally, we discuss the physiological significance of our finding that there is a phenotype of mitochondria-rich cells which coexpresses in the apical membrane a proton-ATPase and an exchange system for small anions.

The External Proton Concentration Gradient

The unstirred layer. At the surface of a membrane exposed to a well stirred solution the lateral rate of solute flow is zero, and close to the surface of the membrane there will be a layer of solution which is almost stagnant. In this so-called unstirred layer, diffusion of solutes is more important than convection for mixing. As a purely operational parameter, the thickness of the unstirred layer, δ, can be defined according to (see, e.g., Dainty, 1963; Dainty and House, 1966; Andersen, 1978; Pedley, 1983; Barry and Diamond, 1984):

$$\left(\frac{dC}{dy}\right)_{surface} = \frac{C_{bulk} - C_{surface}}{\delta}, \qquad (1)$$

where C with subscripts denotes concentration in bulk solution (bulk) and on the surface of the membrane (surface), respectively, and y is the vertical distance from the surface perpendicular to the membrane; $(dC/dy)_{surface}$ is the derivative of the concentration profile at the interface between membrane and solution. The thickness of the unstirred layer depends on the physical properties of the surface and the stirring rate of the surrounding medium. At the mucosal surface of

frog skin mounted in chambers of different perfusion rates, the thickness of such a layer varied from 30 to 60 μm (Dainty and House, 1966) to no more than 12 to 15 μm (fast flow; Lindemann et al., 1972); in other membrane systems δ varied from 50 to 500 μm (Andersen, 1978; House, 1981). We have no independent measurements of δ, and we cannot apply Eq. 1 since, as we show later, the stationary concentration profile is not linear in the presence of a buffer in the unstirred layer. However, given the slow mucosal perfusion rate and the geometric properties of the epithelial surface at the site of measurement (see Fig. 1 *A*), we expect δ to attain higher values (e.g., 200–500 μm) than the above listed for the frog skin. In our theoretical treatment concerning the estimation of proton pumping rates we show that the nonlinear proton concentration profile is not caused by a "stirring" effect, but rather by the chemical reaction taking place between protons and buffer molecules in the unstirred layer. We furthermore depict an empirical way to estimate the thickness of the unstirred layer in our experiments.

Mitochondria-rich cell density. The density of epidermal MR-cells (D_{MRC}) of *B. bufo* kept under our standard laboratory conditions (MATERIALS AND METHODS) exhibits a significant variation ranging from $\sim 10^4$ to $\sim 10^5$ MR cells per cm^2, with an average density of $\sim 6 \times 10^4$ MR cells per cm^2 (Willumsen and Larsen, 1985; Budtz et al., 1995). Assuming a uniform distribution of MR cells in a quadragonal grid, the distance, d (in μm), between two adjacent MR cells is given by, $d = 10^4 \cdot (D_{MRC})^{-1/2}$. Thus, for $D_{MRC} = 6 \times 10^4$ MR cells cm^{-2}, $d = 41$ μm.[3]

Calculation of external proton concentration profiles. It would be possible to localize H^+-pumping MR cells if the tip of the H^+-sensitive microelectrode could be placed on the apical membrane of individual cells. If the distance between neighboring MR-cells is large (i.e., D_{MRC} is small), we would be able to distinguish MR cells with H^+-pumps from principal cells with no H^+-pumps even at a considerable distance from the epithelial surface. With an increasing distance from the epithelial surface, and/or an increasing number of point sources, local $[H^+]$-profiles vanish. To study this relationship in a more rigorous way, a mathematical model of diffusion from a multitude of point sources is analyzed in APPENDIX A. First, we assume 122,500 identical point sources distributed in a quadragonal grid on a plane surface. This model represents a preparation with surface area 2 cm^2 having a typical density of MR cells, which all expresses functional proton pumps. Sample calculations based on this model are presented in Fig. 11 *A* showing the proton concentration as a function of the position (x) in the horizontal plane. Horizontal concentration profiles were computed for different vertical distances (y) above the membrane with x and y normalized to the same value, i.e., the distance between two neighboring point sources. It is seen (Fig. 11 *A*) that at any vertical distance, $y \geq 0.1$, the horizontal concentration fluctuations are vanishingly small. With a distance between two MR cells of 30–50 μm (see above), $y = 0.1$ would be close to the thickness of the cornified layer. Thus, the theoretical calculations confirm what was experimentally observed: with the tip of the microelectrode just above the surface of the preparation, the measured proton concentration is essentially identical above all cells and independent of whether the tip is positioned near an MR cell or a principal cell. Our calculations also indicate that even for $y = 0.01$ (an absolute distance of 0.3–0.5 μm), the horizontal concentration fluctuations remain undetectable with a pH-sensitive microelectrode (Fig. 11 *A*, *right side y-axis*).[4]

The number of sources in the model has a significant effect on the horizontal concentration-fluctuations. To illustrate the general nature of this point, let $F_C(y)$ indicate the normalized function of the maximum amplitude of the horizontal fluctuations, with y, as above, being the normalized distance from the plane containing the sources. Thus, $F_C(y)$ is calculated as the difference between the maximum and minimum concentration, for a given value of y, relative to the concentration, C_0, taken at a fixed set of coordinates on the plane, $y = 0$ (see APPENDIX A, Eq. A7, and Fig. A2). In Fig. 11 *B*, $F_C(y)$ is given for different values of N, where $4N^2$ is the total number of point sources considered. Trivially, independent of N, $F_C(y) \to \infty$ for $y \to 0$, since the concentration above a true point source increases with the reciprocal of the distance from the source. Of more interest, Fig. 11 *B* also illustrates how $F_C(y)$ increases as N in the model is reduced. In the following, we will use the information provided by this family of relationships to discuss conditions which have to be fulfilled for resolving the position of individual point sources with a microelectrode. With the actual noise level of our experimental setup we can detect a change of the microelec-

[3]For this calculation we could as well assume that the MR cells are distributed in a pattern of regular hexagons with a cell in the center of each hexagon. For this geometry, $d = 10^4 \cdot [2 \cdot (3)^{1/2} \cdot D_{MRC}]^{-1/2} = 10746 \cdot (D_{MRC})^{-1/2}$, which with the above example would lead to a distance of 44 μm. Actually measured distances between two neighboring MR cells show a very significant variation within the same preparation. In some areas d is no more than 5 μm (estimated from photos of the epithelial surface with silver-stained MR cells). This reflects that MR cells are not uniformly distributed over the skin surface but have a tendency to cluster (e.g., Fig. 1 *B*).

[4]The model presented here does not take into account the effect of external pH-buffers. Besides that of the external bath, fixed anion residues in the layer of cornified cells might constitute a buffer with a certain (unknown) capacity. However, a fixed buffer in this layer would favor lateral distribution of protons within the layer, which would diminish and not enhance horizontal concentration fluctuations.

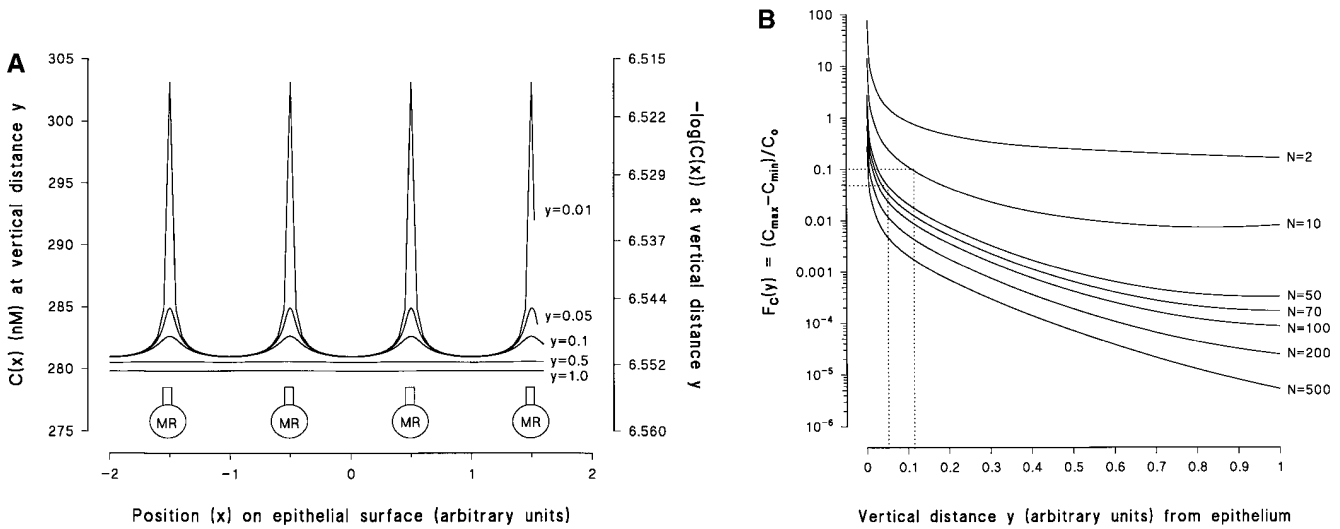

FIGURE 11. (*A*) Predicted variations in horizontal concentration profile obtained at various relative vertical distances (y) above a plane containing 122,500 point sources. At the level of the x-axis four point sources (*MR*) are indicated. (*B*) Family of curves based on the model illustrated in *A*. $F_C(y)$ denotes the relative amplitude of the horizontal concentration fluctuations as a function of the vertical distance y, depicted for different number of point sources ($4N^2$) incorporated. Dashed lines represent $F_C(y)$ values corresponding to the detection limit of our pH-sensitive microelectrode. For details, see text.

trode voltage output of 1–2 mV corresponding to an external pH-amplitude of 0.02–0.04 pH-U. Assuming $C_0 = 282$ nM, it follows that the detection limit of our method corresponds to a value of $F_C(y) = 0.046$–0.096, which in Fig. 11 *B* is indicated by dashed horizontal lines. Thus, as an example, with the microelectrode tip moved horizontally in a plane 2–6 μm from the epithelium ($d = 40$ μm), no more than 400 ($N = 10$) to 10,000 ($N = 50$) point sources must be present for resolving their individual positions. The conclusion is that by monitoring external $[H^+]$-profiles we cannot expect, generally, to identify MR-cells with proton pumps in a flat-type heterocellular epithelium like the skin and the urinary bladder.

Two methods for estimating proton pumping rates. The above analysis also leads to the conclusion that with a large number of "point sources" and provided we consider proton concentrations not too close to the membrane, the total flux of protons can be estimated from a model based on diffusion from a homogenous plate. Thus, a simple approach for calculating the proton flux (J_H) is based on the slope of the tangent of the steady-state $[H^+]$-profile at the interface between the cornified layer and the mucosal bath, e.g., Fig. 3. This approach assumes that close to the epithelial surface the solution is stagnant so that a convection flux of protons and protonated buffer molecules can be disregarded. Thus, from Fick's law (see also LeBlanc, 1971; Demarest and Morgan, 1995):

$$J_H = -D_H \cdot \frac{dC_H}{dy} - D_{BH} \cdot \frac{dC_{BH}}{dy}, \qquad (2)$$

where D_H and D_{BH} are the diffusion coefficients for H^+ and the protonated buffer molecule (Tris), respectively, C_H and C_{BH} are their concentrations, and y is the vertical distance from the outside of the cornified cell layer. The derivative dC_H/dy can be estimated simply as the slope of the tangent at $y = 0$, $(\Delta C_H/\Delta y)_{y=0}$. By insertion of the buffer equation in Eq. 2 and subsequent differentiation, we derive an expression allowing us to calculate the proton flux at the surface (see APPENDIX B):

$$J_H = -\left[D_H + \frac{D_{BH} \cdot C_{TOT} \cdot K_a}{(K_a + C_H)^2}\right] \left.\frac{dC_H}{dy}\right|_{y=0}, \qquad (3)$$

where C_{TOT} and K_a is the total concentration and dissociation constant, respectively, of the buffer. According to a general relationship between diffusion coefficient and molecular weight (Setlow and Pollard, 1962), we assume $D_{BH} \approx 0.7 \times 10^{-5}$ cm$^2 \cdot$ s^{-1}. The slope of the tangent at $y = 0$, $(\Delta C_H/\Delta y)_{y=0}$, was -8.0 ± 3.3 nM $\cdot$ μm^{-1} ($N = 17$) and with $D_H = 9.3 \times 10^{-5}$ cm^2 s^{-1} (H_2O, 25°C, Atkins, 1994) we obtain, $J_H = 8.7 \pm 2.9$ pmol $\cdot$ cm$^{-2} \cdot$ s^{-1}. This method, however, might underestimate the proton flux, because it depends on two measurements only, obtained at $y = 0$ and $y = 50$ μm. It cannot be expected that these two concentrations always provide a precise determination of the slope of the $[H^+]$-profile at $y = 0$ (see Fig. 3).

A more precise method for estimating J_H would be to evaluate Eq. 3 with the boundary values, $C_{H,0}$ and $C_{H,\Delta}$, at $y = 0$ and at $y = \Delta$, respectively (see also McLaughlin and Dilger, 1980; Walter et. al., 1982), thus considering

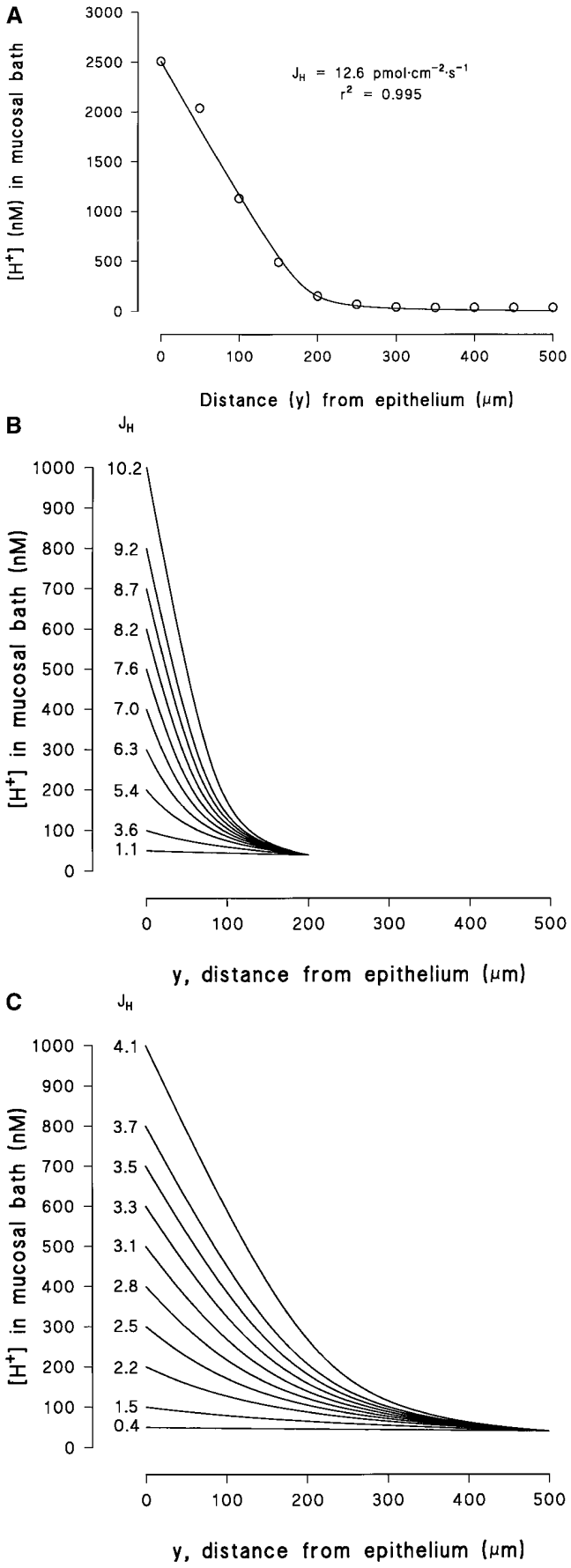

several steady-state pH-values measured at increasing vertical distances in the stagnant layer ($\Delta \leq \delta$). A mathematical model of the stationary $[H^+]$-profile which incorporates one-dimensional diffusion fluxes of protons and protonated buffer molecules is developed in APPENDIX B; in a diffusion regime the proton concentration distribution is given by:

$$C_H(y) = \frac{1}{2} f(y) + \frac{1}{2}\sqrt{f^2(y) + 4\frac{\alpha}{D_H}} - K_a, \qquad (4)$$

where $\alpha = D_{BH} \cdot C_{TOT} \cdot K_a$ and

$$f(y) = C_{H,0} + K_a - \frac{\alpha}{D_H(C_{H,0} + K_a)} - \frac{J_H}{D_H} \cdot y. \qquad (4a)$$

Eq. 4 was fitted to individual $[H^+]$-profiles obtained as indicated in Figs. 2 *B* and 8. All parameters except J_H were fixed, and the fit was optimized by varying J_H from an initial value calculated from Eq. 3. As explained in APPENDIX B, fitting of Eq. 4 to the data points was performed in the layer from $y = 0$ to $y = \Delta$, where Δ is defined as the distance where the theoretical relationship started to deviate systematically from the measurements (as judged by eye; see Fig. 3, *A–C*). The fitted value of the proton flux was, $J_H = 8.5 \pm 2.4$ pmol $\cdot$ cm^{-2} $\cdot$ s^{-1} ($N = 17$, $0.941 \leq r^2 \leq 0.999$).

Fig. 12 *A* shows an example of how Eq. 4 fits measured profiles in experiments with a high $[H^+]$ (pH $\cong$ 5.6) at the epithelial surface. The steep slope observed close to the skin indicates that at this pH there is virtually no buffer capacity (Tris $pK_a = 8.08$). In the absence of a buffer, the steady-state concentration profiles would be linear (Sten-Knudsen, 1978). In the example shown in Fig. 12 *A*, the measured $[H^+]$ appears to be linear within a fairly long distance from the surface of the cornified cell layer. At a distance of 150–200 μm from the surface the buffer becomes effective and, accordingly, the $[H^+]$ approaches that of the bulk solution. Based on Eq. 4, Fig. 12, *B* and *C* depicts the theoretical family of curves with J_H as the adjustable parameter, assuming $\Delta = 200$ and 500 μm, respectively. It is seen that with a relatively high flux and a low Δ (Fig. 12 *B*), we obtain steep concentration profiles with a pronounced shift towards the asymptotic value in the bulk phase, as was observed in Fig. 12 *A*. We consider the fact that Eq. 4 simulates this complex behavior of the $[H^+]$-profile rather well as a verification of the general

FIGURE 12. (*A*) Example of a $[H^+]$-profile fitted by Eq. 4, which was obtained for an acid pH (≅5.6) at the surface. (*B*) The vertical distribution of the proton concentration in the mucosal unstirred layer as predicted by Eq. 4, with J_H as the parameter adjusted, and as an example with a thickness of the unstirred layer (δ) of 200 μm. (*C*) As in *B* but with a δ of 500 μm.

validity of a model describing the effect of a weak buffer in an unstirred layer.

However, not all data sets could be simulated by Eq. 4. Due to a sigmoidal shape of the $[H^+]$-profiles, which could not possibly be simulated by Eq. 4, 6 out of 23 fits were rejected. The sigmoidal profiles might be caused by the permeation of a buffer substance from the epithelium into the aqueous layer adjacent to the surface, or, by local stirring at the surface.

As stated above, Eq. 4 only takes into account the case where diffusion is more important for mixing than stirring. At the distance where stirring becomes the more important factor for mixing, the theoretical line will deviate from the data points. Thus the above described model provides us with an indirect method for estimating the thickness of the unstirred layer (δ), which would be the layer in which the concentration profile is described satisfactorily by Eq. 4, i.e., we assume, $\delta \approx \Delta$. In Fig. 3, *A–C*, are shown results of three different experiments, where the theoretical relationship deviates from the data points at increasing distance from the surface. Based on these fits, we estimate the thickness of the unstirred layer to be 200, 400, and 500 μm, respectively. In our experiments, δ thus estimated varied from 100 to 500 μm with an average of 329 ± 29 μm ($N = 17$). Our measurements indicated, as expected, that by increasing the perfusion rate the pH-gradient was reduced (Fig. 4, *left*). Accordingly, in tissues exhibiting comparable proton fluxes, a relatively small pH-gradient would indicate a relatively fast local perfusion (i.e., effective "stirring") and, thus, a relatively thin unstirred layer. In Fig. 13 the proton concentration at the epithelial surface is depicted as a function of δ, for preparations with comparable proton fluxes (2.2–4.3 pmol · cm^{-2} · s^{-1}). It is apparent that increasing $[H^+]$ is correlated with an increasing unstirred layer thickness (linear regression, $dpH/d\delta \neq 0$, $P < 0.001$, $N = 9$). Since we attempted to keep the macroscopic perfusion constant, other factors such as the position of the microelectrode tip relative to the concavities created by the negative hydrostatic pressure (see Fig. 1 *A*), are likely to have caused variations in δ from experiment to experiment. All pH-measurements were performed when the signal was stationary and, therefore, the vertical movements of the microelectrode tip hardly affected δ at the time of measurement.

The mean mucosal pH-gradient of the 17 data sets considered was 1.03 ± 0.15 pH-U, which is not different either from the mean pH gradient (0.98 ± 0.07) of all 57 preparations studied ($P = 0.76$, $f = 72$), or from the pH-gradient (1.30 ± 0.19) of the 6 rejected fits ($P = 0.32$, $f = 21$). The agreement between the estimates obtained by the simple method, Eq. 3, and the computer based fits, Eq. 4, turned out to be surprisingly good. This is illustrated in Fig. 14, in which the

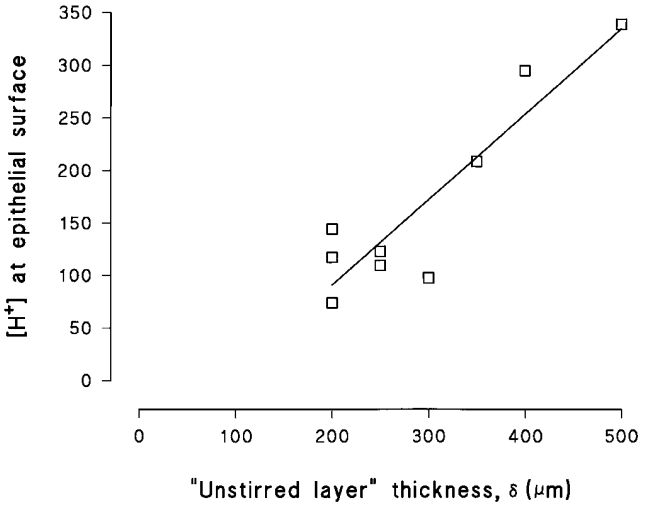

FIGURE 13. Steady-state $[H^+]$ at the epithelial surface as a function of the estimated thickness of the unstirred layer, depicted for preparations with J_H in the range 2.2–4.3 pmol · cm^{-2} · s^{-1}. Linear regression line ($r^2 = 0.83$) with slope different from zero ($P < 0.001$, $N = 9$).

paired J_H-values are plotted against one another. For this set of preparations, the two methods provided statistically similar estimates of J_H ($P = 0.69$, $N = 17$, paired *t* test).

Comparisons with previously published proton fluxes. In previous studies, proton fluxes have been calculated from pH titration and from the short-circuit current in preparations with abolished active Na^+-transport. The proton flux estimated from measured standing mucosal $[H^+]$-gradients, ~8–9 pmol · cm^{-2} · s^{-1}, is comparable to previously measured fluxes in isolated epithelia which ranges from 1 to 9 pmol · cm^{-2} · s^{-1} (Page and Frazier,

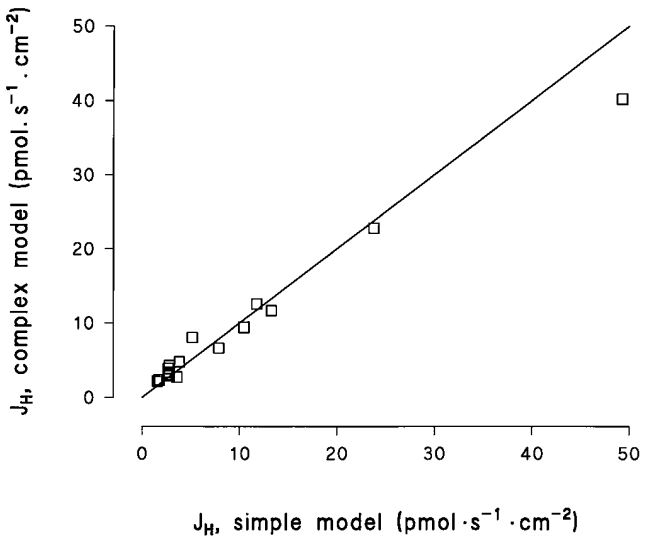

FIGURE 14. Comparison of proton flux estimates based on the simple model, Eq. 3 with flux estimates based on the more complex model, Eq. 4. Full line represents the line of identity.

1987; Harvey, 1992). For reasons which have not been explored, these fluxes by enzymatically isolated epithelia are significantly smaller than those of intact skins which range from 9 to 83 pmol · cm^{-2} · s^{-1} (Emílio et al., 1970; Erlij et al., 1972; Emílio and Menano, 1975; Machen and Erlij, 1975; Ehrenfeld et al., 1985; Page and Frazier, 1987; Ehrenfeld et al., 1989; Yorio et al., 1991; Budtz et al., 1995). By measuring the short-circuit current generated by the proton pump it has been possible to study in detail the relationship between J_H and the $[H^+]$-difference across turtle urinary bladder (Andersen et al., 1985). While the serosal pH was maintained at a constant value of 6.8, the pH in the bulk solution on the well-buffered mucosal side was varied between 9.0 and 4.5. J_H was almost abolished at mucosal pH = 4.5, the flux increased linearly with pH between 4.5 and ~7, and became constant for $7.5 < pH < 9$.[5] In the above mentioned studies on isolated epithelia and intact skin, the measurements of J_H were carried out in a similar range of mucosal pH. Thus, the significantly smaller J_H of isolated epithelia, as compared to intact skins, cannot possibly be due to a lower mucosal pH. Clearly, however, this problem warrants further analysis.

Active Transport of Chloride Driven by a Proton Pump-ATPase

Coupling of proton pump activity and chloride uptake by mitochondria-rich cells. Experiments presented in Fig. 8 and 9 showed that — in a majority of preparations — mucosal acidification was significantly reduced if the poorly permeant gluconate ion is replaced mole for mole by Cl^-. In our previous study (Larsen et al. 1992) this protocol resulted in a complete elimination of the local external $[H^+]$-gradient above MR-cells. These results confirm the earlier finding by Emilio and Menano (1975) that toad skin secretes titratable acid into the external solution in the absence of mucosal Cl^- (SO_4^{2-} replacement), but not in its presence. Thus, the addition of external Cl^-, known to lead to active uptake of this ion, is associated with the secretion of base by MR-cells which partially or fully neutralizes the protons pumped into the mucosal solution by the apical proton-ATPase. The simplest way to account for these observations is to assume expression of the proton-pump and the anion exchanger in the same membrane as depicted in Fig. 15. By coupling the apical uptake of Cl^- to the exit of HCO_3^-, this model also accounts for the observations that the active Cl^- transport is abolished either by application of the carbonic anhydrase inhibitor, acetazolamide (Erlij, 1971; Kristensen, 1972; Bruus et al., 1976), or if serosal pCO_2 is reduced to near zero (Ehrenfeld and Garcia-Romeu, 1978; Larsen et al., 1992). In this context, it is interesting that a polyclonal antibody raised against the band-3 red cell anion exchanger showed a preferential binding to the apical membrane of toad skin MR cells (Katz and Gabbay, 1993). In the model shown in Fig. 15, the exit of Cl^- across the basolateral membrane is assumed to take place by diffusion through channels. This assumption agrees with volume studies of MR cells in situ (Larsen et al., 1987) and finds direct support from a recent patch-clamp study verifying the presence of basolateral Cl^- channels in isolated MR cells (Willumsen and Larsen, 1995). Finally, studies with radio-labeled tracers in whole skin preparations have provided values for the active Cl^- flux of 8–54 pmol cm^{-2} s^{-1} (Martin and Curran, 1966; Erlij, 1971; Kristensen, 1972; Bruus et al., 1976; Ehrenfeld and Garcia-Romeu, 1978; Willumsen and Larsen, 1986; Larsen et al. 1992), which are in satisfactory quantitative agreement with measured proton fluxes in skins of species belonging to the *anura* (see list of proton fluxes in the paragraph above).

Halide selectivity of apical anion exchange. In the present study we have shown that preparations which developed a significant mucosal $[H^+]$-gradient with gluconate in the external bath, but not with Cl^-, in a reversible way also exhibited a significantly reduced gradient in the presence of either Br^- or I^- (Fig. 10). This observation indicates that not only Cl^-, but also other halides may exchange with cellular HCO_3^- of the MR-cells. As a consequence, one would predict that both Br^- and I^- are subjected to transepithelial active transport via the MR-cells, provided that these ions can be translocated through the basolateral anion channels. Indeed,

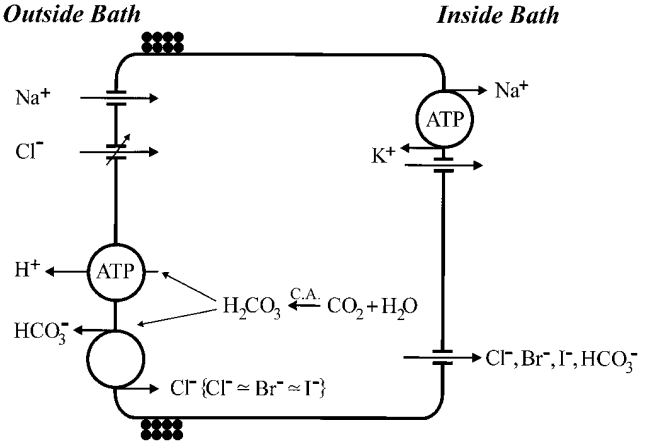

FIGURE 15. Model of the γ-type mitochondria-rich cell of toad skin epithelium. The evidence for apical chloride channels in this cell type is presented by Sørensen and Larsen (1996).

[5]Necessarily, in bladders where $J_H > 0$, the pH in the unstirred mucosal-layer in close proximity of the apical membrane was somewhat smaller than in the bulk-solution. Due to a large mucosal buffer capacity, however, the $[H^+]$-gradient in the unstirred layer of the bladder epithelium is expected to be much less than recorded in the present study.

this is supported by previously published studies. Already Krogh (1937) measured a reduction of the [Br^-] in a diluted bath in which the frog was submersed and he concluded that this ion—like Cl^-—is actively taken up by the skin. Under similar conditions, Krogh did not find evidence of a similar active uptake of I^-. In a much later study of unidirectional tracer fluxes under thermodynamic equilibrium conditions, however, active transport of I^- was unequivocally demonstrated (Harck and Larsen, 1986). In the light of the model of Fig. 15, the findings of the present study (Fig. 10) provide an explanation for the above mentioned earlier observations.

Not All Observations Conform to a Common Model

In several previous studies we and others have measured active Cl^- fluxes and their associated transepithelial currents. Furthermore, in the present series of studies we have examined and compared a large number of preparations with respect to their ability to acidify the mucosal solution in the absence of external Cl^-, and their capacity to excrete base equivalents by a putative Cl^-/HCO_3^- exchanger subsequent to the addition of Cl^- to the mucosal bath. This section serves to provide a comparison of transport features emerging from these studies, which do not seem compatible with the description given above.

Several studies have documented that the isolated skin preparation is capable of active Cl^- uptake and that this flux is rheogenic (Zadunaisky et al., 1963; Bruus et al., 1976; Drewnowska and Biber, 1985; Willumsen and Larsen, 1986; Berman et al., 1987). This set of observations is compatible with the model of Fig. 15, where the apical H^+-pumps and Cl^-/HCO_3^- exchangers in series with basolateral Cl^- channels carry one negative charge across the cell for every Cl^- moved from the outside to the inside solution. We (Dürr and Larsen, 1985) and others (Biber et al., 1980), however, have also published studies where the active Cl^- flux did not generate a transepithelial current. It appears, therefore, that under some conditions a majority of MR-cells expressing Cl^-/HCO_3^- exchangers in the apical membrane does not express proton pumps in this membrane but, rather, in the basolateral membrane. With such a configuration of pumps and exchangers, the MR-cell would still be able to perform active Cl^- transport in the inward direction, but the flux would not carry transepithelial current. Furthermore, unlike the skin in vivo (Jørgensen et al., 1954), under short-circuit conditions the skin of the European frog, *Rana temporaria*, does not exhibit active Cl^- transport and the short-circuit current does not contain any other component than the active Na^+ flux (Ussing and Zerahn, 1951). Possibly, therefore, during isolation the skin loses functioning H^+-pumps and Cl^-/HCO_3^- exchangers. With respect to this possibility, we are also left with the observation that single MR-cells with apical proton pumps have been identified with a pH-sensitive microelectrode and examples have been provided of mucosal [H^+]-profiles approaching resolvable point-sources (Harvey 1992; Larsen et al., 1992). The theoretical analysis presented above indicates that this would not be possible unless the entire preparation contains few, less than 10^4, active point sources. Thus, as in the preparations discussed above, the majority of MR-cells cannot have expressed functional proton pumps. Finally, in 34 out of 43 preparations of the present study, the stationary pH-gradient was reduced in the presence of external Cl^-, whereas in the remaining nine preparations acidification was not reduced or — apparently — it was even stimulated by the addition of Cl^- to the outside solution (Fig. 9). Thus, in these nine preparations which all must have expressed apical proton pumps (due to the existence of a pH-gradient), the majority of MR cells obviously did not express functional Cl^-/HCO_3^- exchangers in the apical membrane.

The transport studies discussed above indicate that there is variation with respect to functional expression of the proton ATPase and anion exchangers as well as with respect to the polarity of their distribution in MR cells in vitro. Little is known about how the expression and the subsequent distribution of these transport systems in MR cells are controlled. Observations discussed above, however, indicate that retrieval, or redistribution, of membrane transporters may occur in connection with isolation of the skin.

Physiological Implications

It is a remarkable property of the amphibian skin that it is capable of transporting sodium and chloride into the body fluid which is 200–500 times more concentrated than the fluid from which these ions are taken up (Krogh, 1937; 1939). Krogh recognized the general importance of his observations by suggesting the existence of active transport mechanisms which couple cellular energy metabolism to the transport of small ions, in casu, sodium and chloride, respectively. The unequivocal proof of active transport was obtained by the introduction of the short-circuiting technique (Ussing and Zerahn, 1951), and subsequent studies with frog skin resulted in the first model of an NaCl transporting epithelium (Koefoed-Johnsen and Ussing, 1958). In this model, the passive flux of Cl^- is driven by the transepithelial electrical potential difference generated by the basolateral Na^+/K^+-pumps. Unlike the short-circuited skin with the relatively high external [NaCl], transport from diluted solutions demands far more energy than can be provided by the Na^+/K^+-ATPase (Larsen et al., 1996). The model shown in Fig. 15 extends the previous model by incorporating MR-cells expressing transport systems for active transport of Cl^-

energized by a proton pump, which is supposed to be in operation when the animal is in the pond. Due to conditions yet to be explored, this function is not maintained in the isolated skin of all species.

APPENDIX A

Mucosal [H^+]-Profiles—Diffusion from Point Sources

To evaluate the influence of a multitude of MR cells to the [H^+]-profile in the mucosal bath, a simple mathematical model is proposed. The model is based on the assumption that the distribution is governed by a steady diffusion process in which each MR cell is represented by a point source. The point sources define a set of particular solutions to Laplace's equation, each contributing to the concentration, $\tilde{C}$, by the expression,

$$\tilde{C} = \frac{Q}{2 \cdot \pi \cdot D} \cdot \frac{1}{\tilde{r}}, \tag{A1}$$

where D [$m^2 \cdot s^{-1}$] is the diffusion coefficient, Q [mol $\cdot$ s^{-1}] is the number of protons leaving the source per unit time, and $\tilde{r}$ [m] is the distance from the source to the point considered. The total concentration at a given point is thus obtained by superposing the contribution from all point sources.

As an example, consider a distribution of sources located equidistantly along a line in the horizontal plane, as shown in Fig. A1. Furthermore, assume that each source contributes with the same strength, i.e., the same Q-value, and they are located with a distance, λ, from each other (in Fig. A1, $\lambda = 1$). The problem may be formulated generally by introducing dimensionless variables as follows,

$$C = \frac{2 \cdot \pi \cdot D \cdot \lambda}{Q} \cdot \tilde{C} \text{ and } r = \frac{\tilde{r}}{\lambda}, \tag{A2}$$

replacing Eq. A1 by the simple expression,

$$C = \frac{1}{r}. \tag{A3}$$

Consider now a coordinate system (X,Y) in which x denotes the horizontal direction, y the vertical direction and the origin is located at the midpoint between the two inner sources (see Fig. A1). The total concentration at a point $P(x,y)$ is obtained by superposing the contribution from each source. We thus get,

$$C(x, y) = \sum_{i=1}^{N} \left[\frac{1}{r_i} + \frac{1}{r_{-i}} \right], \tag{A4}$$

where r_i is the distance from source i to $P(x,y)$. As the distance between two neighboring sources is unity we get,

$$r_i = \sqrt{(|i| - 1/2 - x)^2 + y^2} \text{ and}$$
$$r_{-i} = \sqrt{(|i| - 1/2 + x)^2 + y^2}, \tag{A5}$$

from which the concentration may be determined in all points (x, y). It should be noted that the model is only valid for points not coinciding with the sources, as $C \to \infty$ for $y = 0$ at the points, $x = i - 1/2$, $i = \pm 1, \pm 2, \ldots$ Likewise, at locations above the sources local maxima are found whereas local minima occur in the midpoint between two sources. As a consequence, at a given y-coordinate the concentration exhibits an oscillating behavior as a function of x. At increasing y-values the oscillations damp out, and, for $y >> |N - 1/2 \pm x|$ we get approximately a constant value, $C = 2N/y$.

A more realistic model is straightforwardly formulated by considering $(2N)^2$ sources located evenly in a quadrangular grid, as shown in Fig. A2. Letting (i, k) denote the position of the singularities in the x, z plane, in a coordinate system (X, Y, Z) located in the very center of the grid, the solution reads,

$$C \sum_{i=1}^{N} \sum_{k=1}^{N} \left[\frac{1}{\sqrt{(i - 1/2 - x)^2 + (k - 1/2 - z)^2 + y^2}} + \frac{1}{\sqrt{(i - 1/2 - x)^2 + (k - 1/2 + z)^2 + y^2}} + \frac{1}{\sqrt{(i - 1/2 + x)^2 + (k - 1/2 - z)^2 + y^2}} + \frac{1}{\sqrt{(i - 1/2 + x)^2 + (k - 1/2 + z)^2 + y^2}} \right]. \tag{A6}$$

From Eq. A6 the distribution is calculated in a domain consisting of 122,500 sources ($N = 175$) which corresponds to the expected number of MR cells in a preparation exposing 2 cm^2 in the Ussing chamber. To evaluate the behavior of C-distributions we here con-

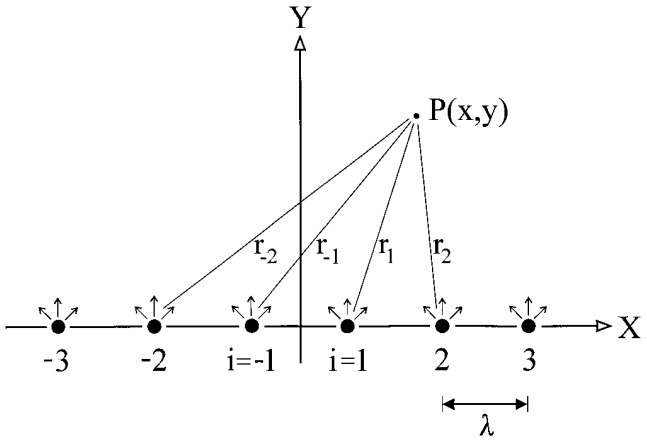

FIGURE A1. Six point sources (i) distributed equidistantly along a line (X). λ indicates distance between two point sources in dimensionless units. Arrows indicate radiary diffusion from each point source. Total concentration in the point $P(x,y)$ is obtained by superposition of the contributions from all point sources.

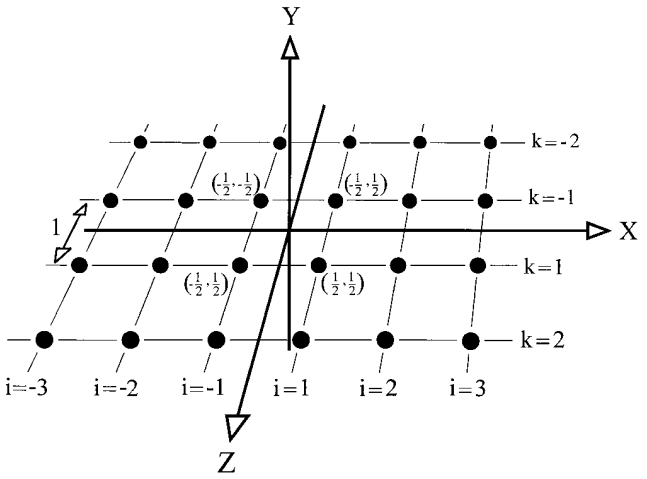

FIGURE A2. Expansion of the model depicted in Fig. A1 into three dimensions. The origin of the coordinate system is located in the point $(x, y, z) = (0, 0, 0)$. Individual point sources are distributed evenly in a quadrangular grid located in the x-z plane at $y = 0$. Numbers in parenthesis are coordinates (x, z) corresponding to a distance of $\lambda = 1$ between neighboring point sources.

sider the fluctuations of C along a line with, z = constant, at different y-coordinates (= vertical distance from the epithelial surface). For simplicity we only consider lines located at $z = 0.5$ in the interval, $x \in [-2, 2]$. Furthermore, as Eq. A6 is in nondimensionalized form we relate it to the present experiment by defining the concentration at $(x, y, z) = (0, 0, 0)$ as the value we measured at the epithelial surface. As this was typically found to be $C_0 = 282$ nM (i.e., pH = 6.55), the C-distribution from Eq. A6 is everywhere multiplied by a factor $C_0/C(x = 0, y, z = 0)$. The outcome in Fig. 11 *A* demonstrates that the concentration (as a function of vertical distance) is dominated by large fluctuations near the epithelial surface (i.e., at small y-values). At increasing distance from the surface the fluctuations are gradually reduced; eventually they vanish. Furthermore, as would also be expected, local maxima appear at positions above the sources (i.e., at $x = -3/2, -1/2, 1/2$, and $3/2$). A general measure of the amplitude of the horizontal C-fluctuations at a given y-location can be expressed as follows,

$$F_c(y) = (C_{max} - C_{min})/C_0, \qquad \text{(A7)}$$

where the maximum value, C_{max}, is obtained just above the source and the minimum value, C_{min}, occurs in the midpoint between two sources (see Fig. 11 *A*). This amplitude, $C_{max} - C_{min}$, is normalized with respect to the concentration, C_0, on the surface at the midpoint between two sources. The quantity, $F_C(y)$ provides a measure of the size of the horizontal fluctuations as a function of the distance from the surface, y, and the number of sources, $4N^2$. It is here expected that increasing the number of sources tends to smooth out the fluctuations and thus decrease $C_{max} - C_{min}$. Considering again (see Fig. A2) the interval, $x \in [-2, 2]$ at $z = 0.5$, we get, $C_{max}(y) = C(x = 0.5, y, z = 0.5)$, $C_{min}(y) = C(x = 0, y, z = 0.5)$, and $C_0 = C(x = 0, y = 0, z = 0.5)$. For this case $F_C(y)$ is depicted in Fig. 11 *B* as a function of distance y and number of sources $4N^2$.

APPENDIX B

Integration of the Flux Equation for Diffusion of Protons

The mathematical treatment of the steady-state mucosal $[H^+]$-profiles incorporates one-dimensional diffusion of protons and protonated buffer molecules (disregarding mixing by stirring). The corresponding flux equation can be written:

$$J_H = -D_H \cdot \frac{dC_H}{dy} - D_{BH} \cdot \frac{dC_{BH}}{dy}, \qquad \text{(B1)}$$

where J_H denotes proton flux, D_H the proton diffusion coefficient, C_H the proton concentration, y the vertical distance from the epithelium, D_{BH} the diffusion coefficient for the protonated buffer, and C_{BH} the concentration of protonated buffer. According to the buffer equation, C_{BH} can be expressed as a function of total buffer concentration (C_{TOT}), proton concentration (C_H), and dissociation constant of the buffer (K_a),

$$C_{BH} = \frac{C_H \cdot C_{TOT}}{C_H + K_a}. \qquad \text{(B2)}$$

Inserting Eq. B2 into Eq. B1 we obtain:

$$J_H = -\frac{d}{dy}\left[D_H \cdot C_H + D_{BH} \cdot C_{TOT} \cdot \frac{C_H}{(C_H + K_a)}\right]. \qquad \text{(B3)}$$

Integrating Eq. B3 from the surface, $y = 0$, into the domain, we get

$$J_H \cdot y = D_H(C_{H,0} - C_H) + \frac{D_{BH} \cdot C_{TOT} \cdot K_a}{(C_{H,0} + K_a)} \cdot \frac{(C_{H,0} - C_H)}{(C_H + K_a)}, \qquad \text{(B4)}$$

where $C_{H,0}$ denotes $[H^+]$ at the surface. It is noted that Eq. B4 is defined only within $y \in [0, \Delta]$, where Δ is a finite distance from the surface such that $\lim C_{y\to\Delta} = C_{H,\Delta}$. From Eq. B4 the concentration is derived as:

$$C_H(y) = \frac{1}{2}f(y) \pm \frac{1}{2}\sqrt{f^2(y) + 4\frac{\alpha}{D_H}} - K_a, \qquad \text{(B5)}$$

where $\alpha = D_{BH} \cdot C_{TOT} \cdot K_a$ and

$$f(y) = C_{H,0} + K_a - \frac{\alpha}{D_H(C_{H,0} + K_a)} - \frac{J_H}{D_H} \cdot y. \qquad \text{(B5a)}$$

In Eq. B5, only the sum of the two terms containing $f(y)$ is physically relevant due to the constraint $C_H(y) \geq 0$.

The steady-state proton flux can be calculated from Eq. B4 by considering that, $C_H = C_{H,\Delta}$ for $y = \Delta$:

$$J_H = D_H \frac{(C_{H,0} - C_{H,\Delta})}{\Delta} + \frac{D_{BH} \cdot C_{TOT} \cdot K_a}{(C_{H,0} + K_a) \cdot (C_{H,\Delta} + K_a)} \cdot \frac{(C_{H,0} - C_{H,\Delta})}{\Delta}. \quad \text{(B6)}$$

This equation requires knowledge of the value of Δ. The difficulty of determining this value, however, led us to use a curve fitting routine for estimating the proton flux. Thus, for finding J_H, Eq. B5 was fitted to the data points in the domain from $y = 0$ to a distance ($y = \Delta$) where the theoretical relationship systematically deviated from the measurements (as judged by eye). Examples of this procedure is demonstrated in Fig. 3, *A–C*, where Δ approximates 200, 400, and 500 μm, respectively. The curve fitting was initiated with a value of J_H obtained by evaluating Eq. B3 at the surface:

$$J_H = -\left[D_H + \frac{D_{BH} \cdot C_{TOT} \cdot K_a}{(K_a + C_H)^2} \right] \frac{dC_H}{dy}\bigg|_{y=0} \quad \text{(B7)}$$

where $dC_H/dy_{(y=0)}$ may be calculated from a simple Taylor expansion. It should be noted that Eq. B7 also has been used to estimate the proton flux (see DISCUSSION).

Thanks are due Mr. Arne Nielsen for construction of mechanical parts and servicing electronic instruments, Mrs. Hanne Schaltz for assistance in preparing isolated epithelia, and Mrs. Birthe Petersen and Mr. Bjarne Brønager for art work.

This study was supported by grants from the Danish Natural Science Research Council (11-0971), the Carlsberg Foundation and the Novo-Nordisk Foundation.

Original version received 27 June 1996 and accepted version received 4 October 1996.

REFERENCES

Al-Awqati, Q. 1992. Cellular and molecular mechanisms of regulation of ion transport in epithelia. *In* The Kidney: Physiology and Pathophysiology. D.W. Seldin and G. Giebisch, editors. Raven Press, New York. 625–644.

Andersen, O.S. 1978. Permeability properties of unmodified lipid bilayer membranes. *In* Membrane Transport in Biology I, Concepts and Models. G. Giebisch, D.C. Tosteson, and H.H. Ussing, editors. Springer Verlag, Berlin/Heidelberg/New York. 369–446.

Andersen, O.S., J.E.N. Silveira, and P.R. Steinmetz. 1985. Intrinsic characteristics of the proton pump in the luminal membrane of a tight urinary epithelium. The relation between transport rate and $\Delta\mu_H$. *J. Gen. Physiol.* 86:215–234.

Atkins, P.W. 1994. Physical Chemistry. Oxford University Press, Melbourne/Tokyo. 1031 pp.

Barry, P.H., and J.M. Diamond. 1984. Effects of unstirred layers on membrane phenomena. *Physiol. Rev.* 64:763–873.

Berman, D.M, M.O. Soria, and A. Coviello. 1987. Reversed short-circuit current across isolated skin of the toad *Bufo arenarium*. *Pflüg. Arch.* 409:616–619.

Biber, T.U.L., T.C. Walker, and T.L. Mullen. 1980. Influence of extracellular Cl concentration on Cl transport across isolated skin of *Rana pipiens*. *J. Membr. Biol.* 56:81–92.

Brown, D., and J.L. Stow. 1996. Protein trafficking and polarity in kidney epithelium: from cell biology to physiology. *Physiol. Rev.* 76:245–297.

Bruus, K., P. Kristensen, and E.H. Larsen. 1976. Pathways for chloride and sodium transport across toad skin. *Acta Physiol. Scand.* 97:31–47.

Budtz, P.E., B.C. Christoffersen, J.S. Johansen, I. Spies, and N.J. Willumsen. 1995. Tissue kinetics, ion transport, and recruitment of mitochondria-rich cells in the skin of the toad (*Bufo bufo*) in response to exposure to distilled water. *Cell Tissue Res.* 280:65–75.

Dainty, J. 1963. Water relations of plant cells. *Adv. Bot. Res.* 1:279–326.

Dainty, J., and C.R. House. 1966. 'Unstirred layers' in frog skin. *J. Physiol. (Lond.).* 182:66–78.

Demarest, J.R., and J.L.M. Morgan. 1995. Effect of buffers on proton secretion from gastric oxyntic cells measured with vibrating ion-selective microelectrodes. *Biol. Bull.* 189:219–220.

Drewnowska, K., and T.U.L. Biber. 1985. Active transport and exchange diffusion of Cl across the isolated skin of *Rana pipiens*. *Am. J. Physiol.* 249:F424–F431.

Dürr, J.E., and E.H. Larsen. 1985. Indacrinone (MK-196): a specific inhibitor of the voltage-dependent Cl^- permeability in toad skin. *Acta Physiol. Scand.* 127:145–153.

Ehrenfeld, J., and F. Garcia-Romeu. 1978. Coupling between chloride absorption and base excretion in isolated skin of *Rana esculenta*. *Am. J. Physiol.* 235:F33–F39.

Ehrenfeld, J., F. Garcia-Romeu, and B.J. Harvey. 1985. Electrogenic active proton pump in *Rana esculenta* skin and its role in sodium ion transport. *J. Physiol. (Lond.).* 359:331–355.

Ehrenfeld, J., I. Lacoste, and B.J. Harvey. 1989. The key role of mitochondria-rich cell in Na^+ and H^+ transport across the frog skin epithelium. *Pflüg. Arch.* 414:59–67.

Emilio, M.G., M.M. Machado, and H.P. Menano. 1970. The production of a hydrogen ion gradient across the isolated frog skin: quantitative aspects and the effect of acetazolamide. *Biochim. Biophys. Acta.* 203:394–409.

Emilio, M.G., and H.P. Menano. 1975. The excretion of hydrogen ion by the isolated amphibian skin: effects of antidiuretic hormone and amiloride. *Biochim. Biophys. Acta.* 382:344–352.

Erlij, D. 1971. Salt transport across isolated frog skin. *Phil. Trans. R. Soc. Lond.* 262:153–161.

Erlij, D., T. Machen, A. Martínez-Palomo, and A. Smith. 1972. Transport across epithelia: structure and function of the outer border of the frog skin. *In* Role of Membranes in Secretory Processes. L. Bolis, R. Keynes, and W. Wilbrandt, editors. North Holland, Amsterdam. 301–309.

Frömter, E. 1988. Mechanisms and regulation of ion transport in the renal collecting duct. *Comp. Biochem. Physiol.* 90A:701–707.

Gluck, S.L., C. Cannon, and Q. Al-Awqati. 1982. Exocytosis regulates urinary acidification in turtle bladder by rapid insertion of H^+ pumps into the luminal membrane. *Proc. Natl. Acad. Sci. USA.* 79:4327–4331.

Gluck, S.L., D.M. Underhill, M Iyori., L.S. Holliday, T.Y. Kostrominova, and B.S. Lee. 1996. Physiology and biochemistry of the kidney vacuolar H^+-ATPase. *Annu. Rev. Physiol.* 58:427–445.

Harck, A.F., and E.H. Larsen. 1986. Concentration dependence of halide fluxes and selectivity of the anion pathway in toad skin. *Acta Physiol. Scand.* 128:289–304.

Harvey, B.J. 1992. Energization of sodium absorption by the H^+-ATPase pump in mitochondria-rich cells of frog skin. *J. Exp. Biol.* 172:289–309.

Harvey, B.J. 1995. Cross-talk between sodium and potassium channels in tight epithelia. *Kidney Int.* 48:1191–1199.

House, C.R. 1981. Unstirred layers and osmotic flow across artificial membranes. *In* Water Transport Across Epithelia*:* Proceedings of Alfred Benzon Symposium. Vol. 34. H.H. Ussing, N. Bindslev, N.A. Lassen, and O. Sten-Knudsen, editors. Munksgaard, Copenhagen. 120–131.

Jørgensen, C.B., H. Levi, and K. Zerahn. 1954. On active uptake of sodium and chloride ions in anurans. *Acta Physiol. Scand.* 30:178–190.

Kaissling, B., and B.A. Stanton. 1992. Structure-function correlation in electrolyte transporting epithelia. *In* The Kidney: Physiology and Pathophysiology, D.W. Seldin and G. Giebisch, editors. Raven Press, New York. 779–801.

Katz, U., and S. Gabbay. 1993. Band 3 protein and ion transfer across epithelia: Mitochondria-rich cells in the amphibian skin epithelium. *Funktionsanalyse Biologischer Systeme.* 23:75–82.

Klein, U., T. Haertel, W. Zeiske, and J. Ehrenfeld. 1995. Identification and location of a V-ATPase in frog skin. *Physiol. Zool.* 68:P197.

Koefoed-Johnsen, V., and H.H. Ussing. 1958. The nature of the frog skin potential. *Acta Physiol. Scand.* 42:298–308.

Kristensen, P. 1972. Chloride transport across isolated frog skin. *Acta Physiol. Scand.* 84:338–346.

Krogh, A. 1937. Osmotic regulation in the frog (R. esculenta) by active absorption of chloride ions. *Skand. Arch. Physiol.* 76:60–74.

Krogh, A. 1939. Osmotic regulation in aquatic animals. Cambridge University Press, Cambridge. 154–162.

Larsen, E.H. 1991. Chloride transport by high-resistance heterocellular epithelia. *Physiol. Rev.*71:235–283.

Larsen, E.H., B.C. Christoffersen, L.J. Jensen, J.B. Sørensen, and N.J. Willumsen. 1996. Role of mitochondria-rich cells in epithelial chloride uptake. *Exp. Physiol.* 81:525–534.

Larsen, E.H., H.H. Ussing, and K.R. Spring. 1987. Ion transport by mitochondria-rich cells of toad skin. *J. Membr. Biol.* 99:25–40.

Larsen, E.H., N.J. Willumsen, and B.C. Christoffersen. 1992. Role of proton pump of mitochondria-rich cells for active transport of chloride ions in toad skin epithelium. *J. Physiol. (Lond.).* 450: 203–216.

LeBlanc, O.H., Jr. 1971. The effect of uncouplers of oxidative phosphorylation on lipid bilayer membranes: carbonylcyanide *m*-chlorophenylhydrazone. *J. Membr. Biol.* 4:227–251.

Lindemann, B., U. Gebhardt, and W. Fuchs. 1972. A flow chamber for concentration-step experiments with epithelial membranes. *T.-I.-T. J. Life Sci. (Oxford).* 2:15–26.

Machen, T., and D. Erlij. 1975. Some features of the hydrogen (ion) secretion by the frog skin. *Biochim. Biophys. Acta.* 406:120–130.

Martin, D.W., and P.F. Curran. 1966. Reversed potentials in isolated frog skin II. Active transport of chloride. *J. Cell. Physiol.* 67: 367–374.

McLaughlin, S.G.A., and J.P. Dilger. 1980. Transport of protons across membranes by weak acids. *Physiol. Rev.* 60:825–863.

Page, R.D., and L.W. Frazier. 1987. Morphological changes in the skin of *Rana pipiens* in response to metabolic acidosis. *Proc. Soc. Exp. Biol. Med.* 184:416–422.

Pedley, T.J. 1983. Calculation of unstirred layer thickness in membrane transport experiments: a survey. *Q. Rev. Biophys.* 16:115–150.

Rosen, S., and N.J. Friedley. 1973. Carbonic anhydrase activity in *Rana pipiens* skin: biochemical and histochemical analysis. *Histochemistry.* 36:1–4.

Setlow, R.B., and E.C. Pollard. 1962. Molecular Biophysics. Addison-Wesley Publishing Company, Inc. Reading, MA. 545 pp.

Sten-Knudsen, O. 1978. Passive transport processes. *In* Membrane Transport in Biology I, Concepts and Models. G. Giebisch, D.C. Tosteson, and H.H. Ussing, editors. Springer Verlag, Berlin/ Heidelberg/New York. 5–113.

Steinmetz, P.R. 1986. Cellular organization of urinary acidification. *Am. J. Physiol.* 251:F173–F187.

Sørensen, J.B., and E.H. Larsen. 1996. Heterogeneity of chloride channels in the apical membrane of isolated mitochondria-rich cells from toad skin. *J. Gen. Physiol.* 108:421–433.

Ussing, H.H., and K. Zerahn. 1951. Active transport of sodium as the source of electric current in the short-circuited isolated frog skin. *Acta Physiol. Scand.* 23:110–127.

Walter, A., D. Hastings, and J. Gutknecht. 1982. Weak acid permeability through lipid bilayer membranes. Role of chemical reactions in the unstirred layer. *J. Gen. Physiol.* 79:917–933.

Willumsen, N.J., and R.C. Boucher. 1992. Intracellular pH and its relationship to regulation of ion transport in normal and cystic fibrosis human nasal epithelia. *J. Physiol. (Lond.).* 455:247–269.

Willumsen, N.J., and E.H. Larsen. 1985. Passive Cl^- currents in toad skin: potential dependence and relation to mitochondria-rich cell density. *In* Transport Processes, Iono- and Osmoregulation. R. Gilles and M. Gilles-Baillien, editors. Springer-Verlag, Berlin/Heidelberg. 20–30.

Willumsen, N.J., and E.H. Larsen. 1986. Membrane potentials and intracellular Cl^- activity of toad skin epithelium in relation to activation and deactivation of the transepithelial Cl^- conductance. *J. Membr. Biol.* 94:173–190.

Willumsen, N.J., and E.H. Larsen. 1995. Chloride channels in the basolateral membrane of mitochondria-rich cells of toad skin epithelium. *J. Physiol. (Lond.).* 489:116*P.*

Yorio, T., R.D. Page, and L.W. Frazier. 1991. Prostaglandin regulation of H^+ secretion in amphibian epithelia. *Am. J. Physiol.* 260: R866–R872.

Zadunaisky, J.A., O.A. Candia, and D.J. Chiarandini. 1963. The origin of the short-circuit current in the isolated skin of the South American frog *Leptodactylus ocellatus. J. Gen. Physiol.* 47:393–402.